

CONFIDENTIAL

Copy 6
RM L55K17



NACA

RESEARCH MEMORANDUM

OSCILLATING HINGE MOMENTS AND FLUTTER CHARACTERISTICS OF A
FLAP-TYPE CONTROL SURFACE ON A 4-PERCENT-THICK UNSWEPT
WING WITH LOW ASPECT RATIO AT TRANSONIC SPEEDS

By Robert F. Thompson and William C. Moseley, Jr.

Langley Aeronautical Laboratory
Langley Field, Va.

CLASSIFIED DOCUMENT

This material contains information affecting the National Defense of the United States within the meaning of the espionage laws, Title 18, U.S.C., Secs. 793 and 794, the transmission or revelation of which in any manner to an unauthorized person is prohibited by law.

**NATIONAL ADVISORY COMMITTEE
FOR AERONAUTICS**

WASHINGTON

February 23, 1956

CONFIDENTIAL

NATIONAL ADVISORY COMMITTEE FOR AERONAUTICS

RESEARCH MEMORANDUM

OSCILLATING HINGE MOMENTS AND FLUTTER CHARACTERISTICS OF A
FLAP-TYPE CONTROL SURFACE ON A 4-PERCENT-THICK UNSWEPT
WING WITH LOW ASPECT RATIO AT TRANSONIC SPEEDS

By Robert F. Thompson and William C. Moseley, Jr.

SUMMARY

Free-oscillation tests were made in the Langley high-speed 7- by 10-foot tunnel to determine the dynamic hinge-moment characteristics of a trailing-edge flap-type control surface on a 4-percent-thick unswept wing with low aspect ratio. The 25-percent-chord control was essentially full span and had an overhang nose balance. Controls with ratios of trailing-edge thickness to hinge-line thickness of 0.17 and 1.00 were tested at angles of attack of 0° and 6° . Tests were made over a Mach number range of 0.60 to 1.02 for control oscillating amplitudes to 10° and for a range of reduced frequencies (based on the semichord of the control) which varied from about 0.05 to 0.16 at the low test speeds and from 0.08 to 0.13 at the high test speeds. The data were also compared with static tests of the same configuration.

Test results show that the aerodynamic damping coefficient becomes unstable near a Mach number of 0.90 and remains unstable to the maximum speed of this investigation (a Mach number of 1.02). A one-degree-of-freedom flutter of the control surface was associated with these unstable aerodynamic damping moments and the flutter characteristics are presented. Damping coefficients were fairly constant with oscillation amplitude at subsonic speeds but became quite nonlinear with amplitude at transonic speeds. Variations in angle of attack, control trailing-edge thickness, and reduced frequency had little effect on the damping coefficient. The aerodynamic spring-moment coefficients agreed with results from static tests. In addition, good agreement was obtained between test results and results computed by a modified two-dimensional potential-flow theory.

[REDACTED]

INTRODUCTION

A number of studies have been made on the static hinge moments on flap-type control surfaces at transonic speeds. However, a relatively small amount of work has been done in measuring the dynamic hinge moments at these speeds. These data are needed in flutter studies and may also be of considerable importance in the design of servo systems.

In the present investigation, a free-oscillation technique was used to measure the dynamic hinge moments on a wing-control configuration which simulated the 4-percent-thick straight wing that the NACA is currently planning to flight test on the X-1E research airplane. A 1/8-scale model of the outboard 35 percent of the wing semispan was tested. These dynamic hinge-moment data were considered necessary in the evaluation of the control-surface flutter characteristics because a recent investigation (ref. 1) has shown that a flap-type control on an unswept 4-percent-thick wing was susceptible to flutter.

Oscillating hinge moments and associated flutter characteristics are presented for a range of control reduced frequency. The effects of control-surface-oscillation amplitude, angle of attack, and control-surface trailing-edge thickness were investigated over a Mach number range of 0.60 to 1.02. In addition, static hinge moments were obtained for the control with the thickened trailing edge to supplement the static data on the basic control profile reported in reference 2.

SYMBOLS

C_h	control hinge-moment coefficient, $\frac{\text{Hinge moment, ft-lb}}{2M'q}$
M_δ	aerodynamic hinge moment on control per unit deflection, positive trailing edge down, ft-lb/radian
q	free-stream dynamic pressure, lb/sq ft
M'	area moment of aileron area rearward of and about hinge line, ft ³
c	local wing chord, ft
c_a	control chord (distance from hinge line rearward to trailing edge of control, see fig. 1), ft

[REDACTED]

- c_b balance chord (distance from hinge line forward to leading edge of control, see fig. 1), ft
- c_t total control chord at midspan of control ($c_b + c_a$), ft
- k reduced frequency, $\frac{\omega c_t}{2V}$
- ω angular frequency of oscillation, $2\pi f$, radians/sec
- f frequency of oscillation, cycles per second
- f_0 control wind-off natural frequency, cycles per second
- V free-stream velocity, ft/sec
- I moment of inertia of control system, slug-ft²
- λ logarithmic decrement, $\frac{d(\log \delta_1)}{d(\text{time})}$, per second
- δ_1 amplitude of oscillation, degrees to each side of mean
- δ control-surface deflection, measured in a plane perpendicular to control-surface hinge line, positive when control-surface trailing edge is below wing chord plane, radians except as noted
- M effective Mach number over span of model, $\frac{2}{S_1} \int_0^{b/2} c_{M_a} dy$
- S_1 twice wing area of semispan model, sq ft
- b twice span of semispan model, ft
- M_a average chordwise local Mach number
- M_l local Mach number
- y spanwise distance from plane of symmetry, ft
- α angle of attack, deg

T ratio of control-surface thickness at trailing edge to thickness at hinge line

$$C_{h\delta} = \frac{\partial C_h}{\partial \delta}$$

$$C_{h\delta}^* = \frac{\partial C_h}{\partial \left(\frac{\delta c_t}{2V} \right)}$$

$$C_{h\delta, \omega} = \frac{\text{Real part of } M_\delta}{2M'q}, \text{ per radian}$$

$$C_{h\delta, \omega}^* = \frac{\text{Imaginary part of } M_\delta}{2M'qk}, \text{ per radian}$$

} the subscript ω indicates coefficients that are a function of ω

B "bumped" flutter condition, flutter starts when control surface is manually displaced 10° and suddenly released

S "self starting" flutter condition, flutter starts when control surface is released without being manually displaced

MODEL AND APPARATUS

The model was designed so that the internal damping and spring constant of the control system could be varied. This was necessary in order to measure the dynamic hinge moments in addition to the flutter characteristics for a range of control reduced frequency. Model details are given in figures 1 and 2. Photographs are shown in figure 3 and a schematic drawing of the test installation is shown in figure 4. The spanwise variation of stiffness distribution of the control system is given in figure 5. The model used during this investigation was a 1/8-scale model of the outboard 35-percent semispan of the 4-percent-thick wing of the X-1E research airplane. This part of the wing includes the trailing-edge flap-type aileron and was tested as a reflection-plane configuration at transonic Mach numbers in the Langley high-speed 7- by 10-foot tunnel.

Wing Details

The model had an aspect ratio of 1.80, a taper ratio of 0.74, and an NACA 64A004 airfoil section with a modified trailing edge. The portion

of the wing rearward of the 70-percent chord line was modified so that the trailing edge had a constant percentage thickness equal to 0.0036c which is identical to that of the airplane. The wing was constructed with a steel core and a plastic surface. Round holes were drilled through the core perpendicular to the chord plane similar to the method described in reference 3 such that the natural first bending and torsion frequencies of the model were similar to those calculated for the airplane wing. Since the model simulated only the outboard portion of the airplane wing, the model mode shapes would not be expected to simulate the airplane mode shapes. To give an indication of the effects of varying the natural frequencies of the model wing, a massive store was added to the wing tip. Details of this tip store are shown in figures 1 and 2 and in table I. The natural first bending and torsion frequencies of the wing, with and without tip store, are given in table II. These frequencies were obtained with the control clamped at 6.2 inches along the hinge line.

Control System Details

The 0.25c flap-type control extended from the 0.086b/2 model station to the 0.943b/2 model station. An 0.20c_a blunt overhang nose balance extended over the outboard 90 percent of the control span and the control nose gap was unsealed. Control construction consisted of a steel spar and a spruce trailing edge with the entire surface covered with silk. A tungsten insert was distributed in the overhang to statically balance the control about the hinge line and as near as possible to balance each spanwise station. Two control profiles were tested. One profile (fig. 1) was similar to the control that will be on the airplane and had a trailing-edge thickness to hinge-line thickness ratio T of 0.17. The second control profile had a T of 1.0.

The inboard tang of the control extended through the reflection plane to the outside of the tunnel. The tang extension consisted of a damper rod and a torsion spring. The control was mounted by two ball bearings outside the tunnel and a plain bearing at the wing tip. The system was carefully aligned to keep friction to a minimum. Attached to the damper rod was a small armature which rotated in the magnetic field of a reluctance-type pickup to indicate control position and a deflection arm used to apply a step deflection to the control system. A movable clamp was used to vary the length of the torsion spring and hence the natural frequency of the control system. The values of natural frequency given on figure 5 for each clamp position are for the two control profiles tested. The lower natural frequency is for the $T = 1.0$ control. The moments of inertia of the control system with the two controls are given in table III. At a test Mach number of 1.00, the total control-system inertia of the $T = 0.17$ control closely simulates the inertia of the airplane control surface at approximately 45,000 feet pressure altitude.

Damper Details

The internal damping of the control system was varied by means of a viscous-type damper. The damper was a 2.5-inch long split bearing which enclosed the damper rod between the two mounting ball bearings (figs. 3 and 4) and had 0.0035-inch clearance between the damper and damper rod. This space was filled with silicone damping fluid and the damping forces resulted from the shearing of this fluid as the control system oscillated. It was not necessary to seal the ends of the damper since fairly high viscosity fluids were used and fluid leakage was negligible. To vary the damping, fluids having different viscosities were used and care was taken to keep the temperature of the fluid during the course of testing the same as when it was calibrated. Calibration of the damper indicated that the damping coefficient was a function of oscillating frequency and wind-off damping tares were applied at the proper frequency when obtaining aerodynamic equivalent viscous damping coefficients.

Instrumentation

Strain gages were located near the root of the wing to indicate the wing bending and torsion response. Control position was measured by a reluctance-type pickup located at the outboard end of the damper rod. These three quantities along with tunnel dynamic pressure were recorded against time by a recording oscillograph. Dynamic calibration of the recording system indicated accurate response to a frequency of about 500 cycles per second.

TESTS

The tests were made in the Langley high-speed 7- by 10-foot tunnel utilizing the side wall reflection-plane test technique. This technique involves mounting a relatively small model on a reflection plate spaced out from the tunnel wall to bypass the tunnel boundary layer. Local velocities over the surface of the test reflection plate allowed testing to a Mach number of 1.02 without choking the tunnel.

Typical contours of local Mach number in the vicinity of the model location, obtained with no model in place, are shown in figure 6. Average test Mach numbers were obtained from similar contour charts using the relationship

$$M = \frac{2}{S_1} \int_0^{b/2} cM_a dy$$

The variation of Reynolds number based on the wing mean aerodynamic chord with test Mach number is presented in figure 7. The width of the band on figure 7 represents, for these tests at a given Mach number, the maximum variation of Reynolds number with atmospheric conditions.

Oscillating hinge moments were obtained for the two control profiles through a Mach number range of 0.60 to 1.02, angles of attack of 0° and 6° , and oscillating amplitudes up to 10° . The reduced frequency k range tested varied from about 0.05 to 0.16 at the low test Mach numbers and from about 0.08 to 0.13 at the high test Mach numbers. In addition, static hinge moments were obtained for the control with the thick trailing edge ($T = 1.0$). Static hinge moments for the $T = 0.17$ control are published in reference 2.

TEST TECHNIQUE AND REDUCTION OF DATA

Oscillating hinge moments were obtained from the free oscillation of the control system after the control had been displaced approximately 10° and suddenly released. The control system was displaced by a hand-operated deflection mechanism and the oscillation frequency at a given Mach number was varied by changing the length of a torsion spring by means of a movable clamp. A schematic drawing of the test installation is shown in figure 4. The tests were made in the following manner. Wind-off motion records were made before and after the wind-on tests of each model configuration. Wind-on tests were made with the damper removed from the system until a flutter condition was encountered. The flutter characteristics were then determined and damping added to the control system to make it stable. The aerodynamic damping in the unstable or flutter range was then determined from the oscillation response of the system with the damper installed. For each record, the inphase and damping moments were determined from the frequency of oscillation and the variation of amplitude with time. It was assumed that the damping forces considered in this investigation were adequately described by an equivalent viscous damping.

To obtain spring- and damping-moment coefficients from tests of this type, it is necessary that the control-system response be essentially that of a single-degree-of-freedom system. Although the stiffness (fig. 5) and inertia distribution (table III) of the control system indicate the possibility of response as a higher order system, oscillograph records (fig. 8) indicated that the control system responded predominantly in one mode. For the range of control-system characteristics tested, the frequency of the aileron wind-up mode (i.e., torsional frequency of the aileron outboard of the position pickup) was equal to or greater than four times the frequency of the actual system response mode indicating that for response at the lower mode frequency, the amplitude contribution of the wind-up mode would be negligible. In addition, an analysis of the

control-system response characteristics by means of an analog computer substantiated this result and showed that the amplitude of the control surface could be accurately indicated by a position pickup located on the damper rod. Thus it was concluded that for the oscillation conditions tested, the control system could be adequately treated as a single-degree-of-freedom system.

The hinge moment existing on an oscillating control is not necessarily in phase with the control surface position and may be represented in complex notation by the relation

$$\frac{M_{\delta}}{2M'q} = C_{h\delta,\omega} + ikC_{h\dot{\delta},\omega} \quad (1)$$

The part $C_{h\delta,\omega}$ is the component in phase with control position and is commonly called the in-phase or spring moment. The part $kC_{h\dot{\delta},\omega}$ is the component that is 90° out of phase with control position, that is, in phase with control velocity, and is commonly called the damping moment. Negative values of $C_{h\delta,\omega}$ oppose the control displacement and hence act as an aerodynamic spring, and result in an increase in the stiffness or an increase in the natural frequency of a control system. Likewise, negative values of $C_{h\dot{\delta},\omega}$ oppose the velocity and hence indicate stable damping; that is, a free oscillation of a control surface with negative values of $C_{h\dot{\delta},\omega}$ would damp out. Positive values of $C_{h\dot{\delta},\omega}$ then would indicate an unstable aerodynamic damping moment, and an oscillation would increase in amplitude unless structural damping or a control system damper provided damping moments greater than the unstable aerodynamic moments. It should be mentioned that frequency effects higher than first order could not be separated by the test method used in this investigation; therefore, the coefficients $C_{h\delta,\omega}$ and $kC_{h\dot{\delta},\omega}$ include the higher order derivatives that are either in phase or 90° out of phase with the control position. The subscript ω is used to indicate hinge-moment coefficients that are functions of control oscillating frequency. Expressions relating the stability coefficients used in equation (1) to commonly used flutter coefficients are given in table IV.

Evaluation of Spring Moments

The aerodynamic inphase or spring moment was determined from the natural frequency of oscillation of the control system. The effects of damping on the natural frequency were considered negligible and, when

possible, frequency measurements were taken from limited amplitude flutter conditions wherein the net damping over a complete cycle was zero. Since the variation of inphase moment is not necessarily linear with amplitude, the values of $C_{h_{\delta, \omega}}$ presented are effective values for the amplitude range of the oscillation. The aerodynamic spring-moment coefficient was determined from the relationship

$$C_{h_{\delta, \omega}} = \frac{I\omega_0^2 - I\omega^2}{2M'q} \quad (2)$$

where the subscript o signifies a wind-off condition.

Evaluation of Damping Moments

The variation of damping moment with oscillating amplitude was obtained by plotting the logarithm of the amplitude of successive cycles of the oscillation against time and taking, at a particular amplitude, the slope of the faired curve through the points as the value of the

logarithmic decrement $\lambda = \frac{d(\log \delta_1)}{d(\text{time})}$ of the oscillation at that amplitude. The aerodynamic damping-moment coefficient was determined from the relationship

$$C_{h_{\delta, \omega}} = \frac{2IV}{qM'c_t} (\lambda - \lambda_0) \quad (3)$$

where the λ subscript o refers to wind-off values taken at the same frequency as the wind-on values.

Determination of Static Hinge Moments

Static hinge moments were measured for the $T = 1.0$ aileron by applying a torque to the aileron system at the damper rod (fig. 5) and recording the output of the position pickup. The static hinge-moment coefficient C_h was determined from the relationship

$$C_h = \frac{\text{Torque, ft-lb}}{2M'q} \quad (4)$$

CORRECTIONS

No corrections have been applied to the data for the chordwise and spanwise velocity gradients or for the effects of the tunnel walls. It is shown in reference 4 that a tunnel resonance phenomenon can appreciably decrease the magnitude of forces and moments measured in oscillation tests. However, it is believed that this phenomenon had no appreciable effect on the results of the present investigation. In general, most of the test frequencies were well removed from the calculated resonant frequencies and there was no apparent decrease in moments for the test frequencies that were close to resonant frequencies. It is possible that the magnitude of the resonant effects would be relieved by the model tip effects and the nonuniformity of the velocity field in the test section.

Static control-deflection corrections have been applied to the output of the position pickup to give the deflection at the midspan of the control surface. No dynamic corrections were applied to account for the "wind-up" of the control surface since, as indicated in the previous section, this effect was shown to be small for the range of these tests.

RESULTS AND DISCUSSION

Presentation of Data

Varying the wing response motion by adding the tip store affected the control aerodynamic damping coefficient $C_{h\delta, \omega}$ and the flutter characteristics as shown in figure 9. The variation of $C_{h\delta, \omega}$ with oscillating amplitude and the associated flutter characteristics are presented in figures 10 through 13 for the complete range of the investigation. Aerodynamic spring-moment coefficients $C_{h\delta, \omega}$ are presented in figure 14 for all test conditions. Static hinge-moment coefficients for the $T = 1.00$ control are given on figure 15. A comparison of $C_{h\delta}$ and $C_{h\delta, \omega}$ obtained from static and dynamic tests is shown on figure 16. Static data for the $T = 0.17$ control were obtained from reference 1. The effect on $C_{h\delta, \omega}$ and $C_{h\delta, \omega}$ of α and T is shown on figures 17 and 18, respectively. A comparison of the aerodynamic spring- and damping-moment coefficients with theory is shown on figures 19, 20, and 21. Local Mach numbers over the wing surface for various free-stream Mach numbers are shown on figure 22.

General Comments on Data

Damping measurements were not made at very low oscillating amplitudes due to test accuracy. Values given for oscillating and flutter amplitude are to each side of mean. The control floating angle was near zero deflection for most test conditions so that the oscillating and flutter amplitudes correspond closely to the control amplitude measured relative to the wing-chord plane. For model safety during the determination of flutter characteristics, once a flutter condition was obtained, the control was allowed to flutter only at the Mach numbers presented in the tables on figures 9 through 13. However, if the flutter was a "bumped" condition, (see symbols for definition) a check was made at each 0.01 increment in Mach number for a "self-starting" condition. For example, on figure 10(c) a bumped flutter condition is considered to exist for all Mach numbers from $M = 0.91$ to $M = 0.94$ and a self-starting flutter condition from $M = 0.94$ through $M = 1.02$. Flutter in all cases was a limited amplitude oscillatory condition and was stopped by hand. On figures 9 through 13, a change in line notation from a solid to a broken line indicates a change from stable to unstable damping. Also, for a given f_0 , the oscillation reduced-frequency k changes with a change in aerodynamic spring moment and values of k are given for each Mach number.

Effects of Wing Motion

Figure 8(a) is an oscillograph record of the model response for the $T = 0.17$ control at $M = 0.94$, $\alpha = 0$, and $f_0 = 170$. This record is typical of the decayed oscillation response of the control system and was taken with the damper installed since the aerodynamic damping for this test condition was unstable. The output of the control position pickup was fairly linear and the control position trace indicates the rate of decay from about 10° control deflection. The wing bending and torsion traces are a measure of the wing root bending and torsion stresses. The wing motions indicated by these stresses were small relative to the initial control amplitude. As shown in figure 8(a), the control motions were analyzed in the presence of wing motions. Ideally, it would be desirable to eliminate any wing response when measuring the control oscillating hinge moments; however, this was not practical for these tests. Therefore, to give some indication of the effects of wing motion, the frequency response characteristics of the wing were altered by adding a massive store to the wing tip and testing a control-frequency range such that the wing response to the control forcing function was greatly reduced. An indication of the effects of reducing the wing motion by means of the tip store is shown on figures 8(b), 8(c), 9, and 14(a).

The effect of the tip store on the flutter characteristics is shown by the oscillograph records on figure 8 and the tables on figure 9. Figures 8(b) and 8(c) are records of the bumped flutter condition listed in the tables on figure 9 at $M = 0.90$. The records show that the free oscillation of the first bending and torsion modes of the wing were stable during flutter and that for the steady-state condition the wing is responding to the control forcing function. (Wing natural frequencies are given in table II.) The wing traces for record 8(c) are approximately four times as sensitive as for 8(b) and it can be seen that the wing motion was greatly reduced by the addition of the tip store without an appreciable effect on the control flutter. Flutter occurred in the same Mach number range at approximately the same frequency and amplitude. The change from a bumped to a self-starting flutter condition was not considered a significant effect in view of the similar response once the flutter was initiated. In addition, a logical inspection of the aerodynamic spring moments (both static and dynamic) and the effect on $C_{h\delta, \omega}$ of varying f_0 indicate that the flutter always occurred at the natural frequency of the control system. The flutter was also extremely sensitive to damping. Therefore it was concluded that the flutter was a self-excited oscillation involving only the degree of freedom of control rotation about the hinge line.

The effect of the tip store on $C_{h\delta, \omega}$ and $C_{h\delta, \omega}$ is shown in figures 9 and 14, respectively. The wing response motion was much less in all cases with the tip store, and wing motion had little effect on the control aerodynamic spring moment coefficient $C_{h\delta, \omega}$. Adding the tip store had some relatively large effects on the magnitude of $C_{h\delta, \omega}$ for certain conditions although the general variation of damping coefficient with amplitude and the Mach number at which the damping became unstable were not changed. In addition, some of the differences shown on figure 9 could possibly be due to the aerodynamic effects of flow over the tip store rather than any wing motion effect. There is the possibility, however, that the control damping-moment coefficients presented include some wing motion effects, but the wing motion effects are considered secondary to the overall results.

Damping Moments and Flutter Characteristics

The variation of aerodynamic damping-moment coefficient $C_{h\delta, \omega}$ with oscillating amplitude and associated flutter characteristics for the $T = 0.17$ control at $\alpha = 0^\circ$ is presented in figure 10. Data are presented for the Mach number and wind-off natural frequency f_0 range tested. Since a free-oscillation technique was used, the oscillation reduced frequency k for a given f_0 is a function of the aerodynamic

spring moment and free-stream velocity and increasing the Mach number decreased the k range covered in this investigation. For all values of f_0 tested, $C_{h_{\delta,\omega}}^*$ is stable and fairly constant with oscillating amplitude at the lower test Mach numbers and no flutter was encountered. As the Mach number increased into the transonic range, $C_{h_{\delta,\omega}}^*$ became very nonlinear with oscillating amplitude and an unstable aerodynamic damping condition existed for most amplitudes from a Mach number of about 0.90 to the maximum speed of the investigation ($M = 1.02$), figure 10. Control-surface flutter was associated with the unstable damping and the flutter characteristics for various Mach numbers are given in the tables. When comparing the flutter characteristics with the damping values, it should be remembered that a certain level of structural damping was present during flutter. (The control system wind-off structural damping ranged from 1 to 3 percent of critical damping.) In the flutter Mach number range, $C_{h_{\delta,\omega}}^*$ generally reached a maximum unstable level at some intermediate amplitude and became less unstable at the higher test amplitudes. Flutter would therefore build up in amplitude until a steady-state condition was reached, wherein, the aerodynamic energy fed into the oscillation over a complete cycle was equal to the energy dissipated by structural damping. Decreasing f_0 from 202 to 0 (figs. 10(a) through 10(e)) had a relatively small effect on the general variation or magnitude of $C_{h_{\delta,\omega}}^*$ with oscillating amplitude or Mach number; however, the flutter condition changed from bumped to self starting at the higher test Mach numbers. This result is difficult to evaluate since damping data were not obtained at very low amplitudes; however, the general level of damping above about 1° amplitude was not affected and therefore the change in flutter condition was not considered significant. The shift in $C_{h_{\delta,\omega}}^*$ from stable to unstable values as the Mach number increases is also shown by plotting maximum unstable values of $C_{h_{\delta,\omega}}^*$ over the amplitude range tested in figures 17 and 18. The variation of damping coefficient with reduced frequency is shown in figures 19 and 20. The spread in $kC_{h_{\delta,\omega}}^*$ shown in figures 19 and 20 between two symbols at the same reduced frequency, indicates the variation in magnitude over the oscillation amplitudes tested. Constant values of $C_{h_{\delta,\omega}}^*$ would fall along a radial line from the origin and it is shown that the general level of $C_{h_{\delta,\omega}}^*$ is fairly constant for the reduced-frequency range of this investigation at both subsonic and sonic speeds. Increasing the angle of attack to 6° had little effect on the general variation of $C_{h_{\delta,\omega}}^*$ with oscillating amplitude or Mach number (figs. 11 and 17).

Increasing the control surface trailing-edge thickness is known to have a large effect on static hinge moments, reference 5. In addition, references 6 and 7 have considered the wing boundary layer to have an important part in a feedback phenomenon leading to transonic control-surface flutter. Therefore, the control trailing-edge thickness was made equal to the hinge-line thickness and the effects on the dynamic hinge moments determined. The damping results at $\alpha = 0^\circ$ and 6° are given in figures 12 and 13. The inertia of the control system was increased when the control trailing edge was thickened and hence the control wind-off natural frequencies changed. Increasing the trailing-edge thickness did not change the general variation of $C_{h_{\delta,\omega}}$ with either amplitude (figs. 10 and 12) or Mach number (fig. 18). As shown in figure 18, there was a very small stable shift in $C_{h_{\delta,\omega}}$ due to thickening the trailing edge; however, the aerodynamic damping was still unstable above a Mach number of about 0.90 and the control flutter characteristics were about the same as for the $T = 0.17$ control. Increasing the angle of attack to 6° also had little effect on the damping or flutter characteristics of the $T = 1.0$ control.

The variation of $C_{h_{\delta,\omega}}$ with Mach number obtained in this investigation is in qualitative agreement with data obtained on trailing-edge flap-type controls on swept and delta wings. A portion of the data from these and the present investigation is presented in reference 8.

Spring Moments

The aerodynamic inphase or spring-moment coefficients $C_{h_{\delta,\omega}}$ obtained in this investigation are given in figure 14. Since the variation of C_h with δ is not necessarily linear, effective values of $C_{h_{\delta,\omega}}$ are given for the oscillation amplitude tested. The reduced frequency for each data point on figure 14 is given on the corresponding damping curves in figures 10 through 13. To provide a comparison, the static variation of C_h with δ was determined for the $T = 1.0$ control and results are presented in figure 15. Static data for the $T = 0.17$ control had previously been reported in reference 1. A comparison of $C_{h_{\delta}}$ and $C_{h_{\delta,\omega}}$ as determined from static and dynamic tests is shown in figure 16. As near as possible, these results were averaged over the same amplitude range. For both static and dynamic tests, the spring-moment coefficient was negative throughout the Mach number range and there was a negative increase in the transonic speed range. As indicated in figures 14, 16, 20, and 21, the effects of reduced frequency on the aerodynamic spring-moment coefficient $C_{h_{\delta,\omega}}$ were small for the range of

these tests. Static values of $C_{h\delta}$ are shown at $k = 0$ in figures 19 and 20. The effect of increasing the trailing-edge thickness is in agreement with static tests in that increasing T shifted $C_{h\delta,\omega}$ in a negative direction for all test Mach numbers, figure 18. The good agreement between static and dynamic tests indicates that static hinge-moment data can be satisfactorily used to compute flutter frequencies for the type of transonic control-surface flutter encountered in this investigation. Also shown in figure 18 is a small stabilizing shift in aerodynamic damping due to increasing T . This indicates that in the flutter Mach number range there was a stabilizing shift in the phase angle of the resultant-moment vector as the trailing edge is thickened. However, this effect on the damping and therefore the flutter is small.

Changing the angle of attack from 0° to 6° had little effect on the aerodynamic spring-moment coefficient $C_{h\delta,\omega}$ for the range of this investigation, figures 14 and 17.

Theory

To date, theoretical studies of the moments on oscillating control surfaces have been based on two-dimensional potential flow and for the investigations in which control coefficients have been tabulated, the control has been hinged at the leading edge. The effects of finite span, airfoil thickness, and shocks have generally been neglected and the assumption of small perturbations is usually made. However, these theoretical studies could be expected to give a reasonably close simulation to the actual flow field for the thin wing of this investigation at $\alpha = 0^\circ$. The theory would not account for the effects leading to the nonlinearities with control amplitude shown for the test results; however, a comparison with theory is of interest.

All theoretical results were computed so as to compensate for the aerodynamic balance on the test control. Values at subsonic speeds were computed from reference 11 for a 30-percent-chord control hinged at the leading edge and then modified by an experimental correction to effectively shift the hinge line rearward the proper amount. The experimental correction was based on the assumption that the phase angle of the resultant control-moment vector was not changed by overhang balance and that the length of the vector was decreased, due to balance, in the same proportion as static tests have shown. The correction was obtained from control balance results at the proper Mach number in reference 9 which agreed with two-dimensional results on a 9-percent-thick wing at low speeds in reference 10. The correction decreased the length of the resultant vector and hence the damping and spring-moment components about 35 percent at $M = 0.60$ and about 32 percent at $M = 0.80$.

Theoretical values at sonic and supersonic speeds were computed from wing coefficient expressions given in references 12 and 13 assuming that at these speeds the control oscillating forces are not influenced by the wing surface in the upstream direction. Under this assumption, the control oscillating forces would be the same as the forces on an isolated wing, provided a wing axis of rotation position is chosen so as to simulate the control hinge location. Expressions relating the stability coefficients ($C_{h_{\delta,\omega}}$ and $C_{h_{\delta,\omega}^*}$) used in this paper with the coefficients used in the reference papers are given in table IV.

The comparison between test results and theory is given in figures 19, 20, and 21. The quantity $kC_{h_{\delta,\omega}^*}$ was presented in figures 19 and 20 since it is proportional to the moment component that contributes to the damping (see eq. (1)) and thus brings the relative magnitude of the spring- ($C_{h_{\delta,\omega}}$) and damping-moment components into the proper perspective. The phase angle θ of the resultant-moment vector can be obtained from figures 19 and 20 by the relation, $\tan \theta = \frac{kC_{h_{\delta,\omega}^*}}{C_{h_{\delta,\omega}}}$.

The spread in $kC_{h_{\delta,\omega}^*}$ between two symbols at the same reduced frequency, indicates the variation in magnitude over the oscillation amplitudes tested. As shown in figure 19, excellent agreement is obtained at subsonic speeds between the modified theory and $kC_{h_{\delta,\omega}^*}$ and it can be seen that $C_{h_{\delta,\omega}^*}$ is fairly constant for the reduced frequencies of these tests. (Constant values of $C_{h_{\delta,\omega}^*}$ would fall along a radial line from the origin.) Theory also confirms the test results showing that, for the test reduced frequencies, the effect of frequency on the aerodynamic spring moments $C_{h_{\delta,\omega}}$ is very small; however, the modified two-dimensional theory predicts spring moments that are too large. Static values of $C_{h_{\delta}}$ given at $k = 0$ were obtained from reference 1.

It was pointed out in reference 11 that as the frequency approaches zero, the validity of the sonic theory is subject to question. This note of caution appears to be justified as the results shown in figure 20 indicate, that for reduced frequencies less than about 0.12, the sonic theory of reference 11 is inadequate in predicting magnitudes or trends of either damping or spring moments. It is of importance, however, that this idealized theory predicts unstable damping moments in a range in which experiment also shows unstable damping. In addition, theory predicts magnitudes of $C_{h_{\delta,\omega}}$ and $kC_{h_{\delta,\omega}^*}$ reasonably well at the higher

test reduced frequencies. This condition exists in spite of the extreme nonlinearities encountered. Experimental results at sonic speeds vary with reduced frequency in much the same manner as at subsonic speeds except that the damping is unstable. For the reduced frequency range investigated, the effect of frequency on the spring-moment coefficient is negligible and, although the damping varies considerably with amplitude, experimental trends indicate that the general level $C_{h_{\delta, \omega}}$ is also fairly constant. Sonic theory indicates that at reduced frequencies above about 0.17 the aerodynamic damping of the test control would be stable. Unfortunately, the control system stiffness distribution was such that test reduced frequencies high enough to substantiate this result could not be obtained. However, it was found during the course of testing that if the control system stiffness was made somewhat higher than that which gave $f_0 = 202$, the self-starting flutter condition was eliminated at both 0° and 6° angle of attack. However, since it was necessary to clamp the control system at the deflector mechanism for this condition, the control could not be displaced and damping moments on a control oscillating at these high reduced frequencies ($k \geq 0.13$) were not obtained.

Previous investigations on transonic control-surface flutter (refs. 6 and 7) have indicated the possibility that flutter is caused by separation effects with emphasis placed on shock and boundary-layer interaction. In particular, reference 6 has shown one case of flutter to be associated with a fore-and-aft movement of a shock located on the wing ahead of the control. For the present investigation, the chordwise variation of local Mach number over the wing surface is given in figure 22 at $\alpha = 0$ for the $T = 0.17$ control. These results were obtained by static pressure orifices located in the wing surface at the control midspan and indicate that there were no strong shocks ahead of the control surface for the flutter Mach number range of this investigation. There is the possibility of a shock wave located on the control surface which could conceivably have a significant effect on the flutter. This possibility was pointed out for a similar wing-control configuration in reference 1. However, comparison of experimental results of this investigation with potential flow theory shows very good agreement in the trends of aerodynamic damping with Mach number (fig. 21) and an instability is indicated in the transonic speed range which is substantiated by experiment. Similar results for swept and delta wings were shown in reference 8. Therefore there appears to be a strong indication that single-degree-of-freedom, transonic control-surface flutter is dependent on potential-flow effects.

CONCLUSIONS

The results of the investigation at Mach numbers from 0.60 to 1.02 of the oscillating hinge-moment characteristics of a trailing-edge flap-type control surface mounted on a 4-percent-thick wing with low aspect ratio indicate the following conclusions:

1. The aerodynamic damping coefficient of the control surface $C_{h_{\delta},\omega}$ varied from a level of stable damping at Mach numbers from 0.60 to 0.80 to a level of unstable damping for Mach numbers from 0.92 to 1.02 which was the maximum for these tests.

2. A self-starting flutter condition involving only rotation of the control surface about the hinge line was associated with the unstable damping and was eliminated in all cases by making the total damping (structural plus aerodynamic) in the control system stable.

3. For oscillating amplitudes to 10° , the damping coefficient was essentially constant with amplitude at subsonic speeds and became quite nonlinear with amplitude at transonic speeds.

4. Changing the angle of attack from 0° to 6° or increasing the control trailing edge to hinge-line thickness ratio from 0.17 to 1.00 had little effect on the aerodynamic damping coefficient.

5. The aerodynamic inphase or spring-moment coefficient $C_{h_{\delta},\omega}$ varied with Mach number, angle of attack, and trailing-edge-thickness ratio in much the same manner as static tests have shown.

6. For the reduced-frequency range of these tests, frequency had little effect on either the damping or spring-moment coefficients, $C_{h_{\delta},\omega}$ and $C_{h_{\delta},\omega}$.

7. Good agreement was obtained between the test results and results computed by two-dimensional potential-flow theory. This indicates the possibility that the single-degree-of-freedom, transonic control-surface

flutter encountered in this investigation is dependent on potential-flow effects.

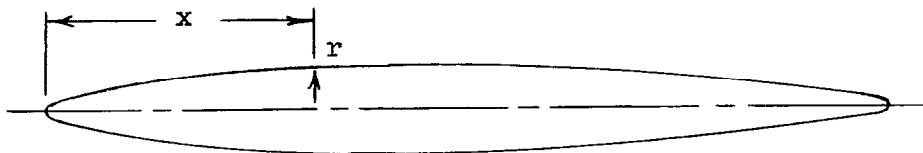
Langley Aeronautical Laboratory,
National Advisory Committee for Aeronautics,
Langley Field, Va., November 10, 1955.

REFERENCES

1. Henning, Allen B.: Results of a Rocket-Model Investigation of Control-Surface Buzz and Flutter on a 4-Percent-Thick Unswept Wing and on 6-, 9-, and 12-Percent-Thick Swept Wings at Transonic Speeds. NACA RM L53I29, 1953.
2. Moseley, William C., Jr.: Investigation at Transonic Speeds of the Hinge-Moment Characteristics of a 1/8-Scale Model of the X-1E Aileron. NACA RM L55F06a, 1955.
3. Land, Norman S., and Abbott, Frank T., Jr.: Method of Controlling Stiffness Properties of a Solid-Construction Model Wing. NACA TN 3423, 1955.
4. Runyan, Harry L., and Watkins, Charles E.: Considerations on the Effect of Wind-Tunnel Walls on Oscillating Air Forces for Two-Dimensional Subsonic Compressible Flow. NACA Rep. 1150, 1953. (Supersedes NACA TN 2552.)
5. Thompson, Robert F.: Investigation of a 42.7° Sweptback Wing Model To Determine the Effects of Trailing-Edge Thickness on the Aileron Hinge-Moment and Flutter Characteristics at Transonic Speeds. NACA RM L50J06, 1950.
6. Erickson, Albert L., and Stephenson, Jack D.: A Suggested Method of Analyzing for Transonic Flutter of Control Surfaces Based on Available Experimental Evidence. NACA RM A7F30, 1947.
7. Biot, M. A., and Arnold, Lee: Investigation of Aileron Compressibility Flutter. Tech. Rep. 6341 (ATI No. 108003), Air Materiel Command, U. S. Air Force, Aug. 1950.
8. Martin, Dennis J., Thompson, Robert F., and Martz, C. William: Exploratory Investigation of the Moments on Oscillating Control Surfaces at Transonic Speeds. NACA RM L55E31b, 1955.
9. Thompson, Robert F.: Hinge-Moment, Lift, and Pitching-Moment Characteristics of a Flap-Type Control Surface Having Various Hinge-Line Locations on a 4-Percent-Thick 60° Delta Wing - Transonic-Bump Method. NACA RM L54B08, 1954.
10. Sears, Richard I.: Wind-Tunnel Data on the Aerodynamic Characteristics of Airplane Control Surfaces. NACA WR L-663, 1943. (Formerly NACA ACR 3108.)

11. Anon.: Tables of Aerodynamic Coefficients for an Oscillating Wing-Flap System in a Subsonic Compressible Flow. Rep. F. 151, Nationaal Luchtvaartlaboratorium, Amsterdam, May 1954.
12. Nelson, Herbert C., and Berman, Julian H.: Calculations on the Forces and Moments for an Oscillating Wing-Aileron Combination in Two-Dimensional Potential Flow at Sonic Speed. NACA Rep. 1128, 1953. (Supersedes NACA TN 2590.)
13. Garrick, I. E., and Rubinow, S. I.: Flutter and Oscillating Air-Force Calculations for an Airfoil in a Two-Dimensional Supersonic Flow. NACA Rep. 846, 1946. (Supersedes NACA TN 1158.)

TABLE I
TIP-STORE ORDINATES
(Percent of store length)



x	r
0	0
1.95	.95
4.72	2.03
7.51	2.88
10.29	3.52
15.85	4.43
21.40	5.04
26.93	5.49
29.73	5.67
32.53	5.80
35.33	5.84
Straight line	
49.73	5.84
52.53	5.81
55.33	5.76
60.93	5.51
66.40	5.13
72.00	4.63
77.60	4.03
83.20	3.35
88.66	2.63
93.73	1.95
96.00	1.63
98.13	1.28
100.00	0
Trailing-edge radius	.56

TABLE II

NATURAL FIRST BENDING AND TORSION FREQUENCIES OF WING

Test condition	Bending, cps	Torsion, cps
Without tip store	119	296
With tip store	56	152

Note: The control surface was clamped when obtaining these frequencies.

TABLE III

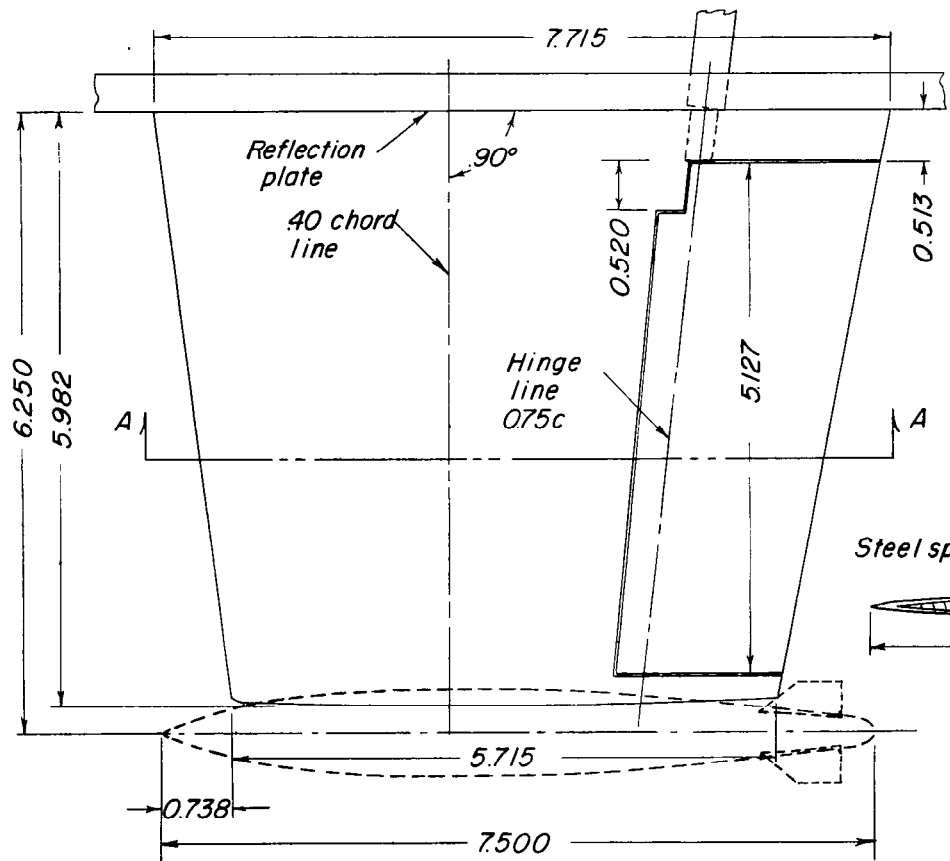
MOMENT OF INERTIA OF CONTROL SYSTEM

Component of System	(slug-ft ²)
Portion of system excluding control surface	3.84×10^{-6}
T = 0.17 control surface	2.50×10^{-6}
T = 1.00 control surface	4.58×10^{-6}

TABLE IV
 EXPRESSIONS RELATING THE STABILITY COEFFICIENTS OF
 THE PRESENT INVESTIGATION TO THE
 FLUTTER COEFFICIENTS USED IN
 REFERENCES 11, 12, AND 13

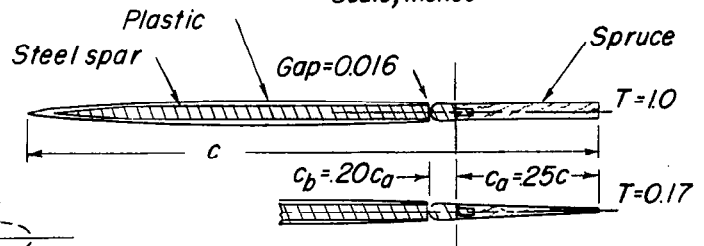
Present paper	Reference 11	References 12 and 13
$C_{h\delta, \omega}$	$\frac{\pi}{2\tau^2} n_c'$	$-\frac{C_a^2 K_a^2 L}{M'} M_3$
$C_{h\dot{\delta}, \omega}$	$\frac{\pi}{2k\tau^2} n_c''$	$-\frac{C_a^2 K_a L}{M'} M_4$

where L is the control span in feet.



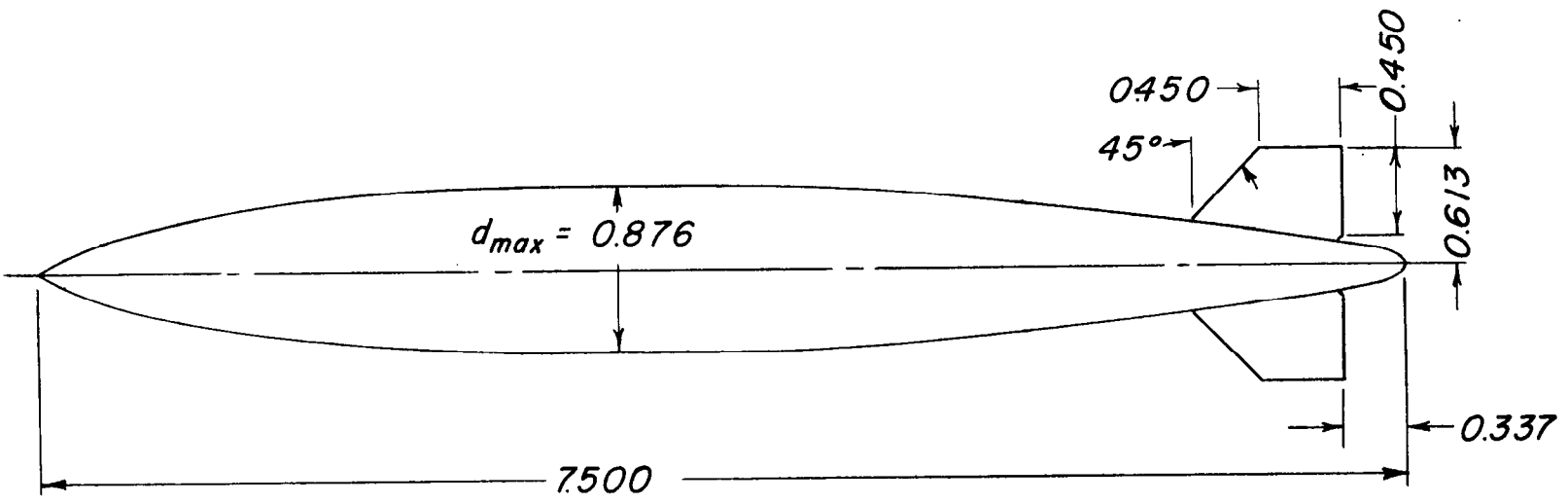
TABULATED WING DATA

Area	0.558 sq ft
Aspect ratio	1.80
Taper ratio	0.74
Mean aerodynamic chord	0.564 ft
Airfoil section parallel to free stream	NACA 64A004 (modified)



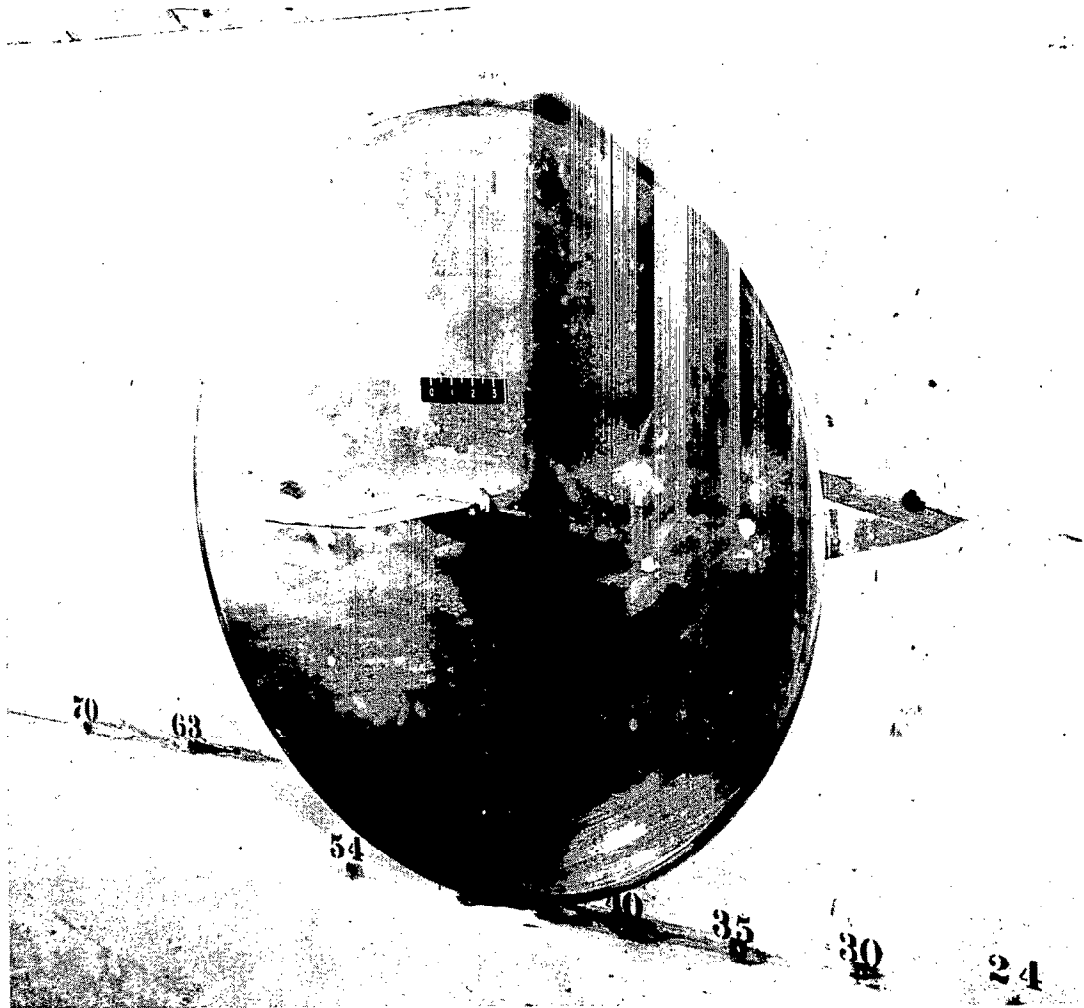
Section A-A
(For two control profiles tested)

Figure 1.- General dimensions of the test model.



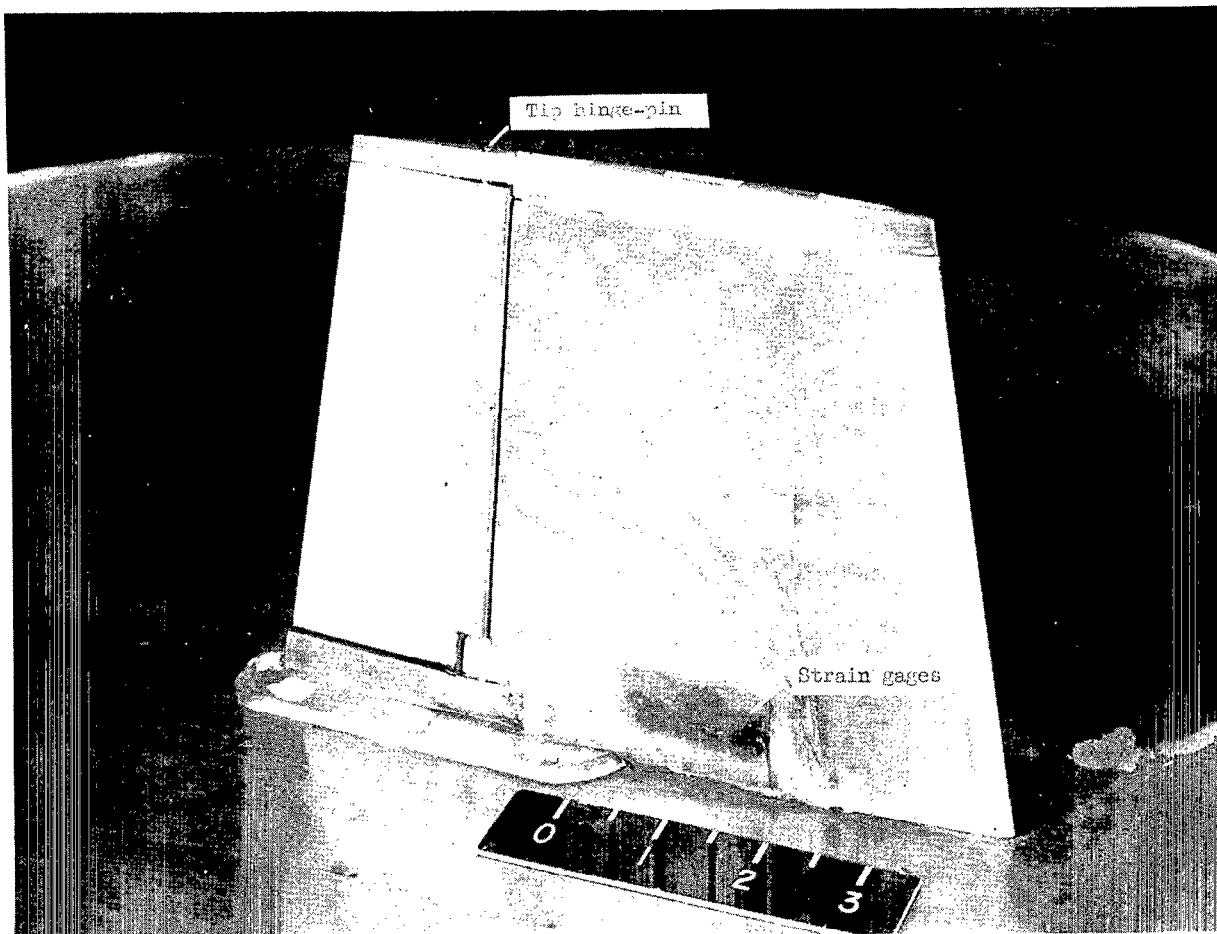
Scale, inches

Figure 2.- Details of tip store.



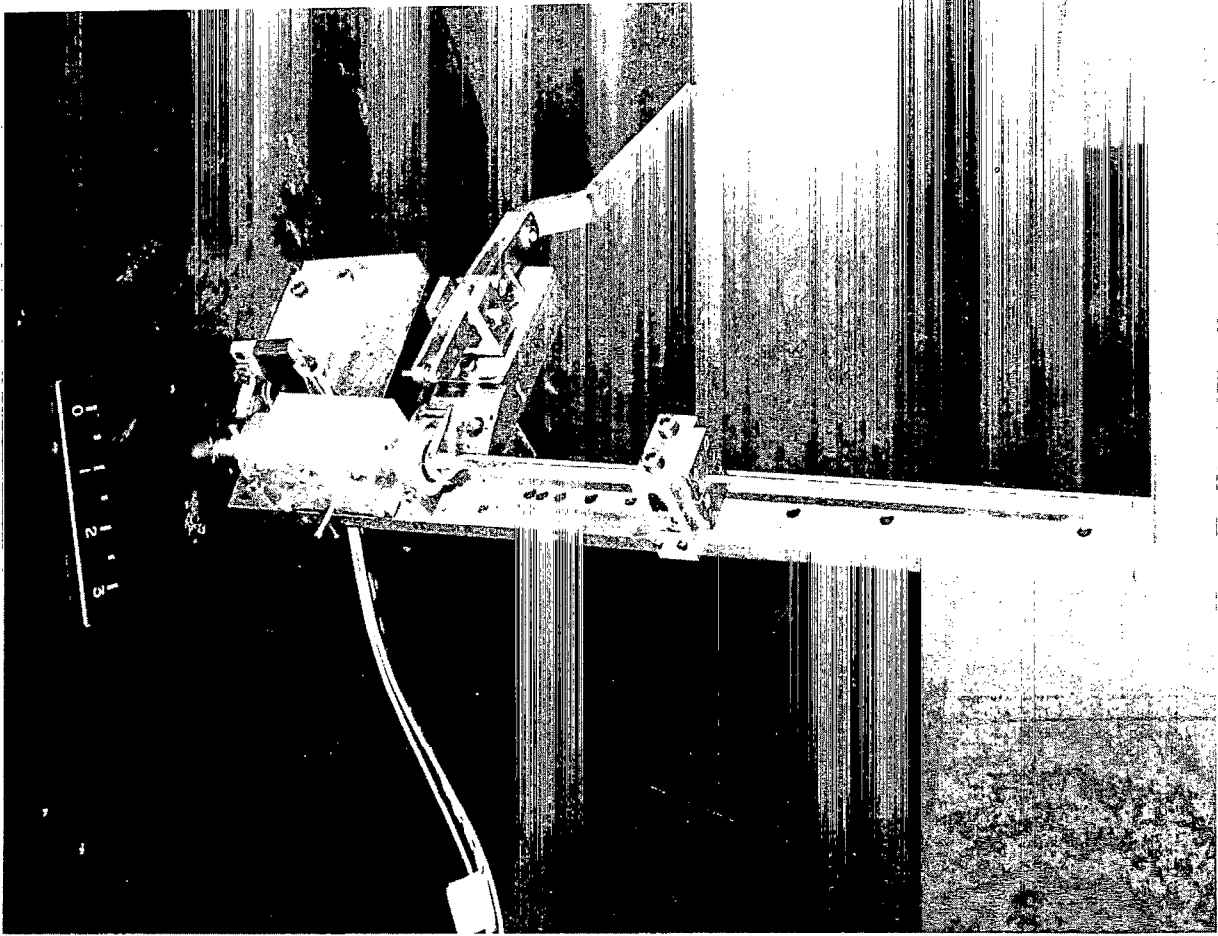
(a) Model and reflection plane mounted in tunnel. L-86715

Figure 3.- Photographs of the model.



(b) Closeup of model showing strain-gage installation. L-86714.1

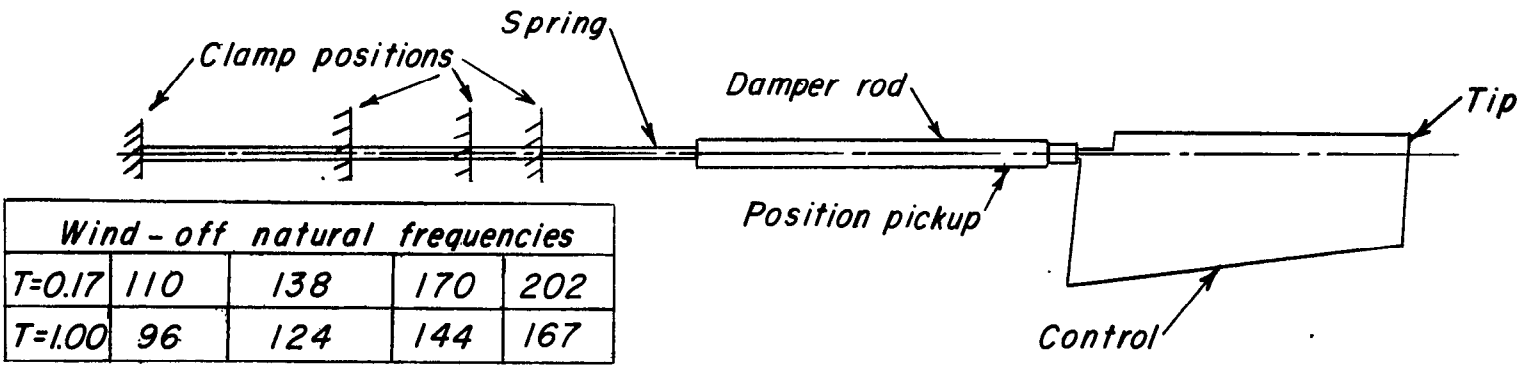
Figure 3.- Continued.



L-87763

(c) Back side of reflection plate showing test components.

Figure 3.- Concluded.



Wind-off natural frequencies				
$T=0.17$	110	138	170	202
$T=1.00$	96	124	144	167

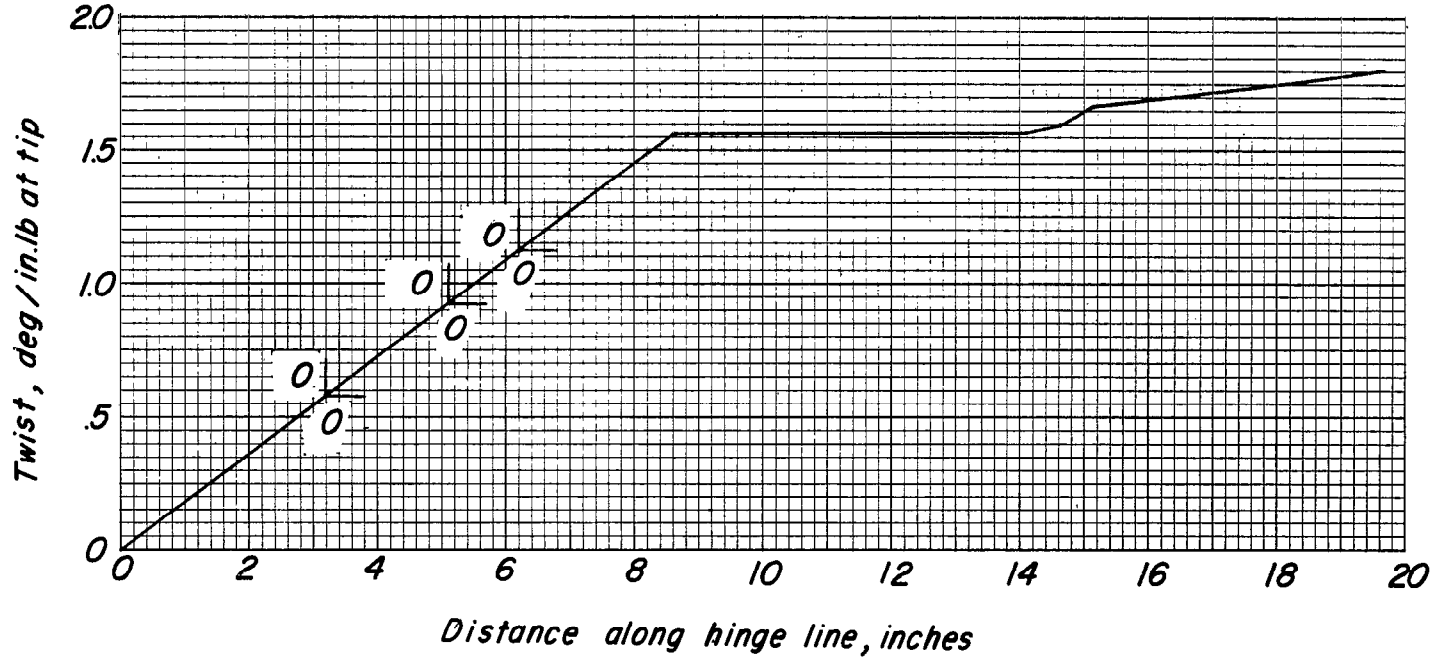


Figure 5.- Frequency and spanwise variation of control-system stiffness for various clamp positions.

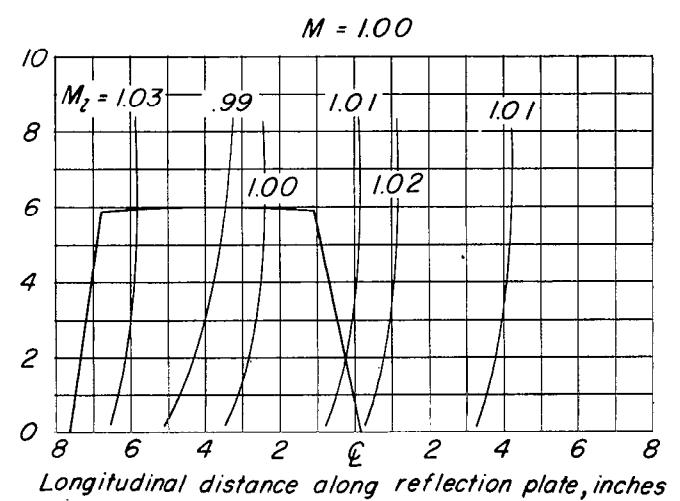
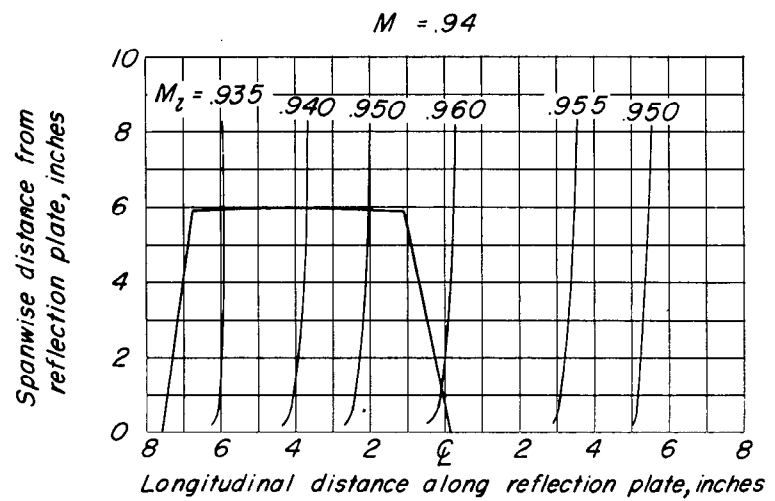
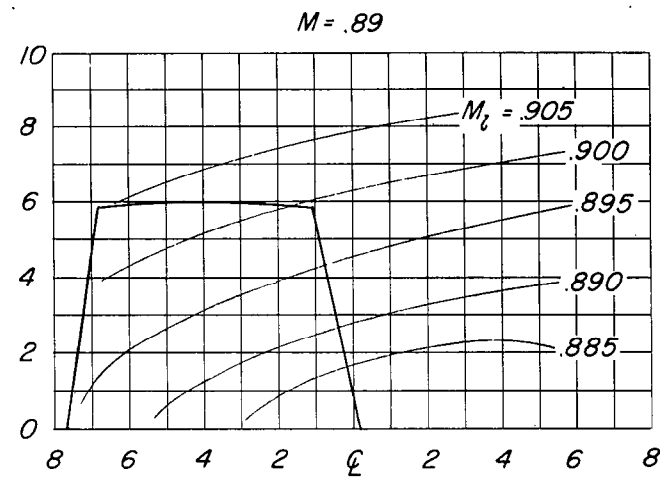
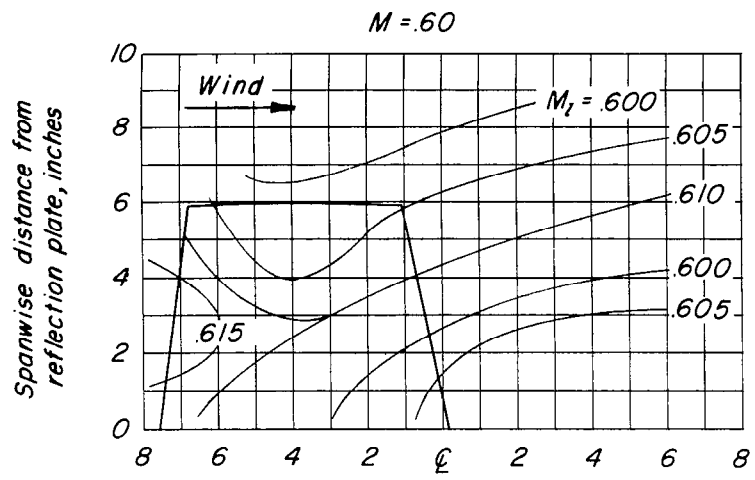


Figure 6.- Typical variation of Mach number contours over the side wall reflection plate with no model in place.

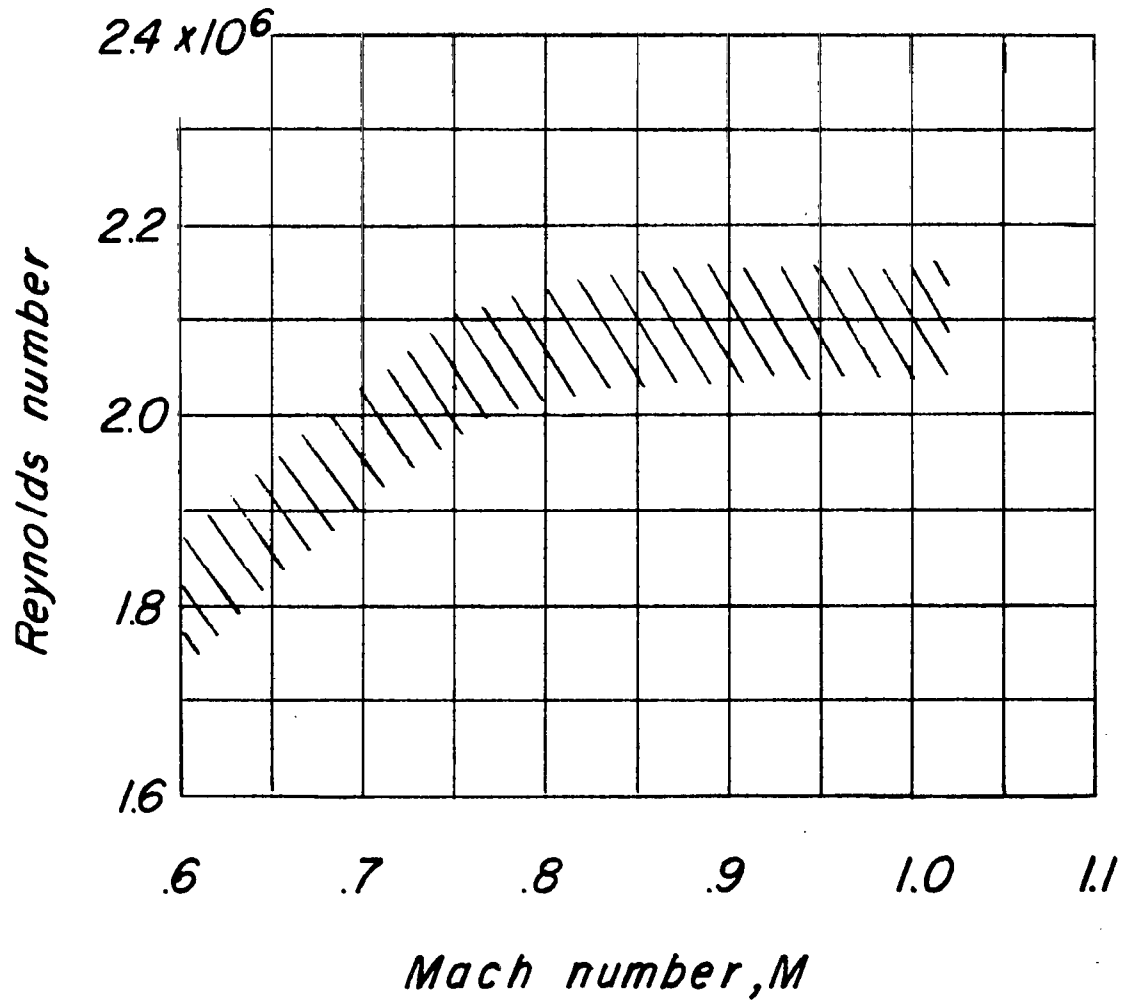
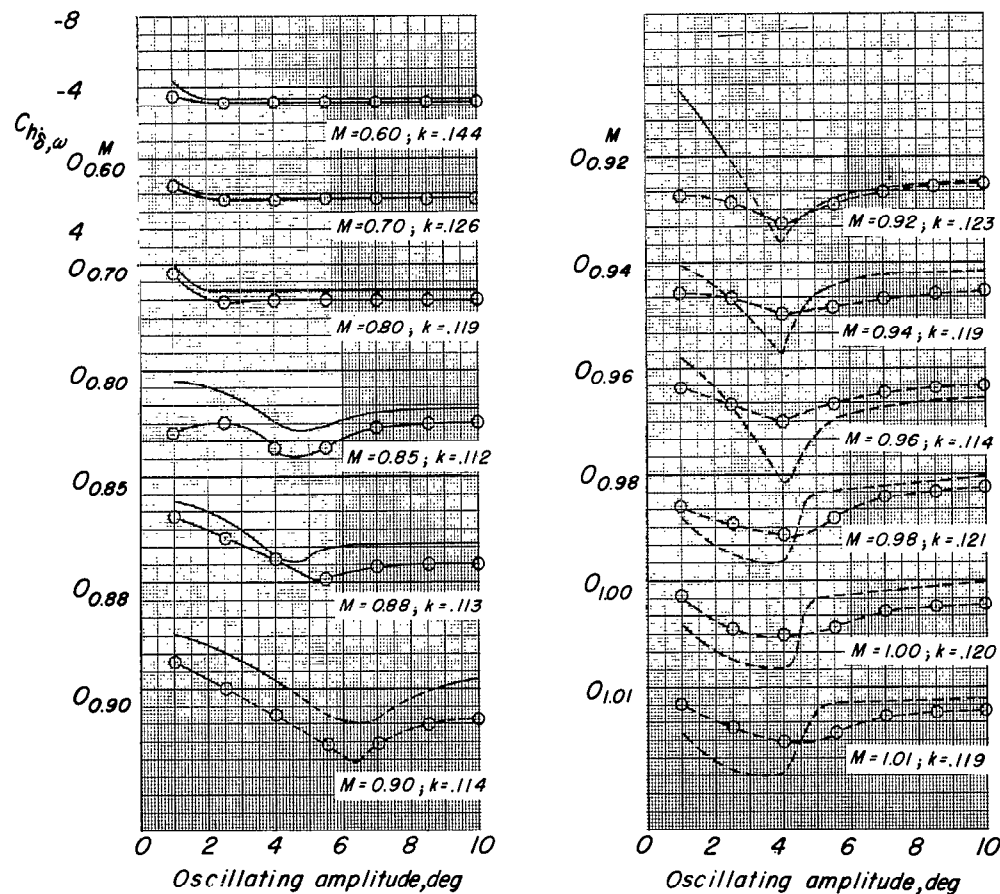


Figure 7.- Variation of test Reynolds number with Mach number.



— Stable
 - - - Unstable

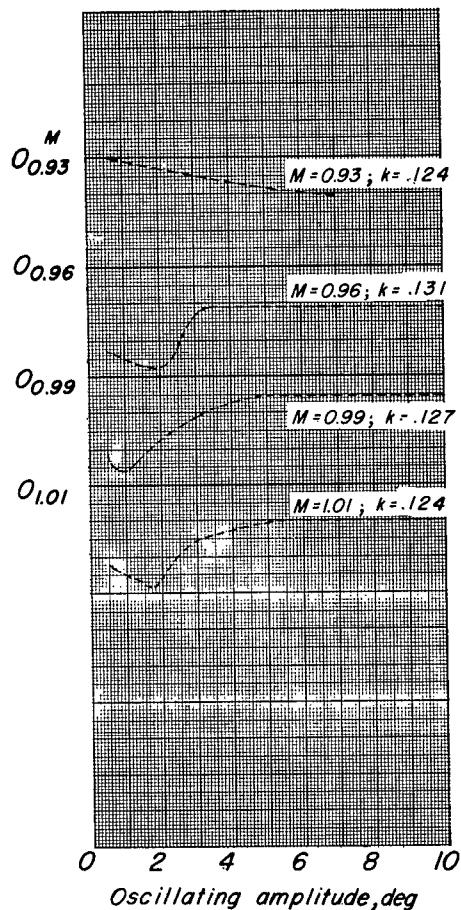
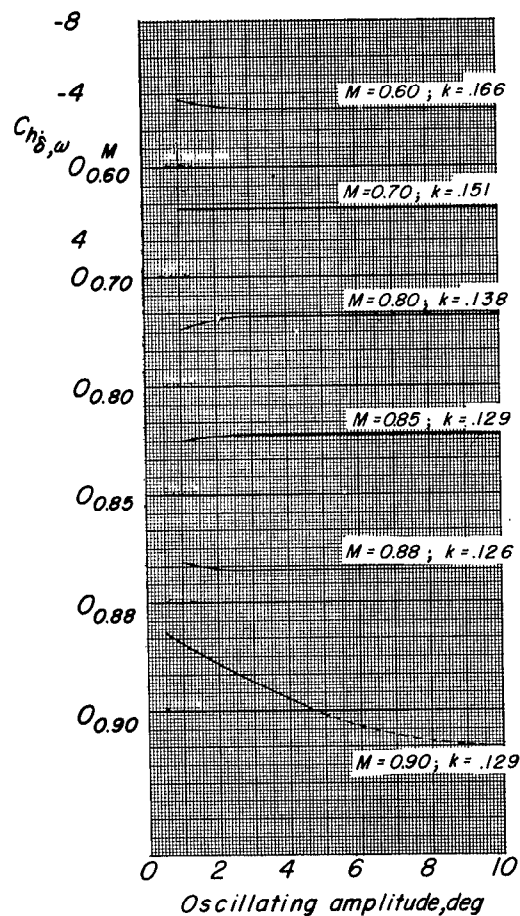
Flutter Characteristics
 (without tip-store)

M	Flutter condition	Frequency cps	Amplitude deg
0.60	No flutter		
0.70	↓		
0.80	↓		
0.85	↓		
0.88	↓		
0.90	B	240	8.2
1.02	B	259	12.0

Flutter Characteristics
 (with tip-store)

M	Flutter condition	Frequency cps	Amplitude deg
0.60	No flutter		
0.70	↓		
0.80	↓		
0.85	↓		
0.88	↓		
0.90	B	234.5	8.9
0.92	S	237	9.6
0.94	S	240	10.1
0.96	S	245	10.8
0.98	S	250	12.1
1.00	S	252	12.3

Figure 9.- Effect of tip store on flutter characteristics and variation of $Ch_{\delta, \omega}$ with oscillating amplitude for various Mach numbers. (Symbols indicate data with tip store.) $f_0 = 170$; $\alpha = 0^\circ$; $T = 0.17$.



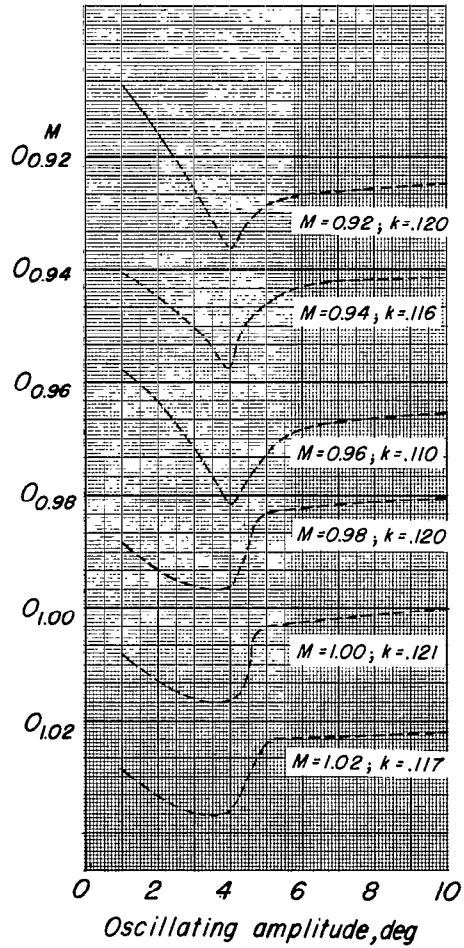
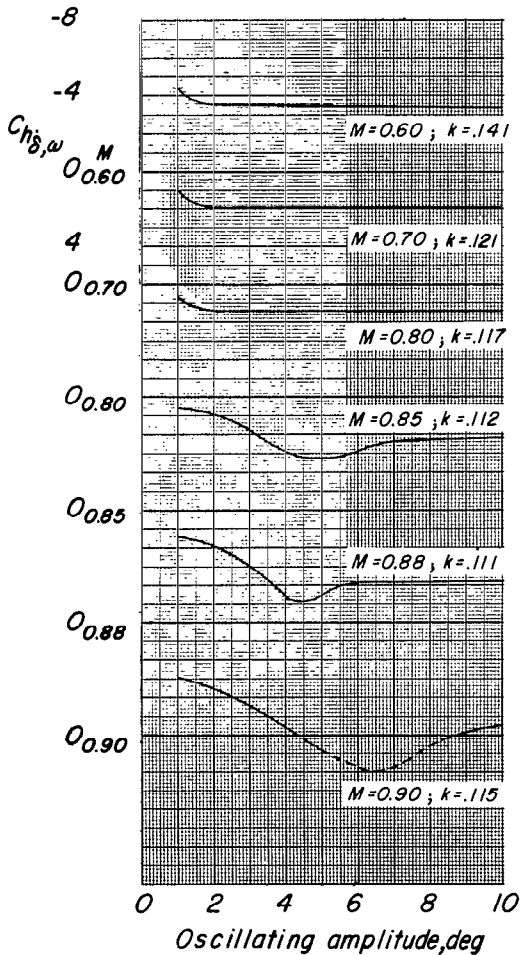
— Stable
 ---- Unstable

Flutter Characteristics

M	Flutter condition	Frequency cps	Amplitude deg
0.60	No flutter		
0.70			
0.80			
0.85			
0.88	↓		
0.90	B	2575	8.2
0.91	B	260	8.7
0.96	B	266.5	11.47
1.02	B	269.0	10.82

(a) $f_0 = 202$.

Figure 10.- Flutter characteristics and variation of $C_{h\delta, \omega}^M$ with oscillating amplitude for various Mach numbers. $\alpha = 0^\circ$; $T = 0.17$.



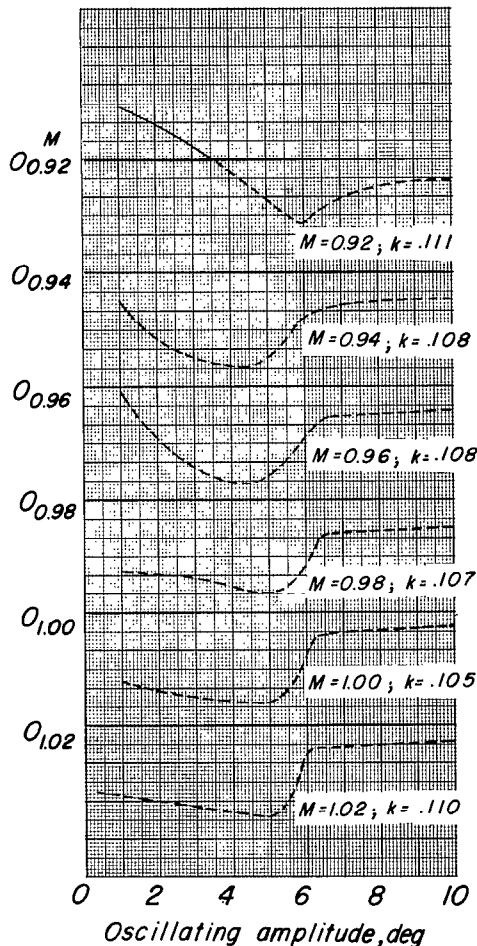
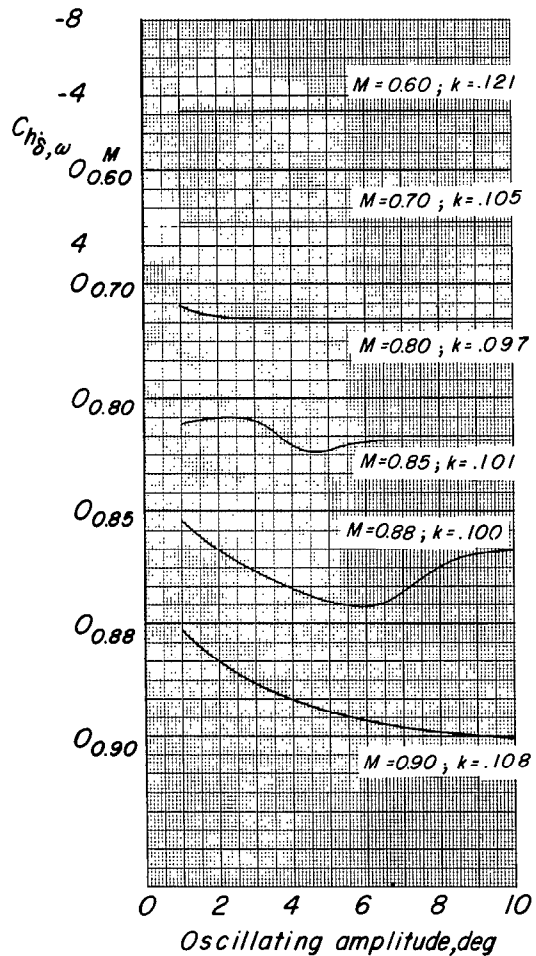
— Stable
 - - - Unstable

Flutter Characteristics

M	Flutter condition	Frequency cps	Amplitude deg
0.60	No flutter		
0.70			
0.80			
0.85			
0.88	↓		
0.90	B	240	8.2
1.02	B	259	12.0

(b) $f_0 = 170$.

Figure 10.- Continued.



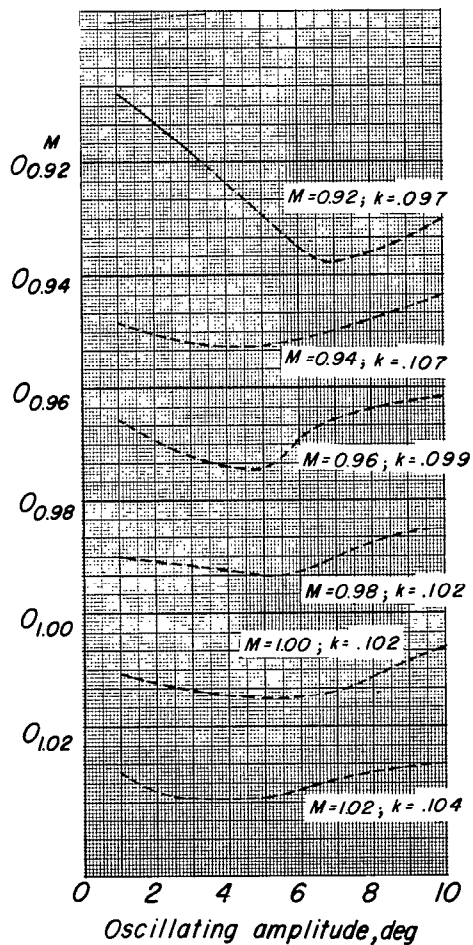
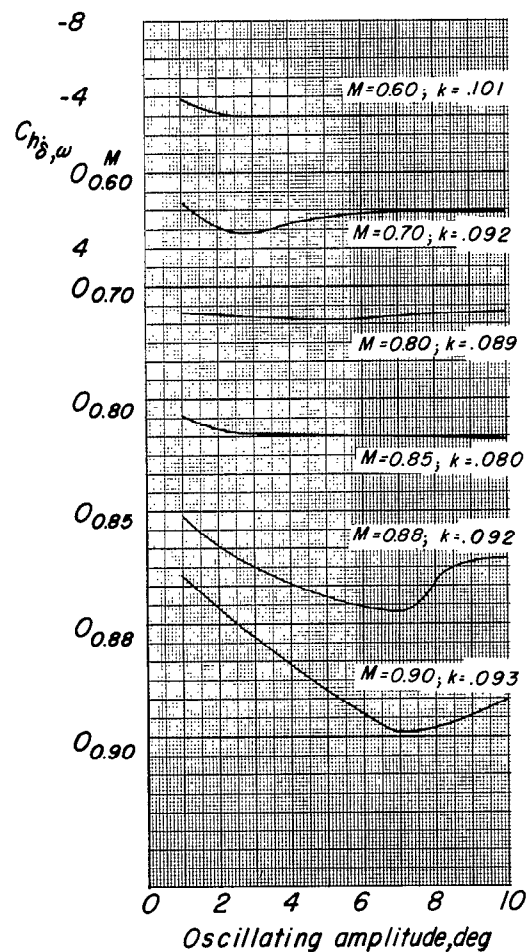
— Stable
 - - - Unstable

Flutter Characteristics

M	Flutter condition	Frequency cps	Amplitude deg
0.60	No flutter		
0.70	↓		
0.80			
0.85			
0.88			
0.91	B	217.5	10.0
0.94	S	233	13.2
0.98	S	233	13.0
1.00	S	233	12.5
1.02	S	233.5	13.0

(c) $f_0 = 138$.

Figure 10.- Continued.



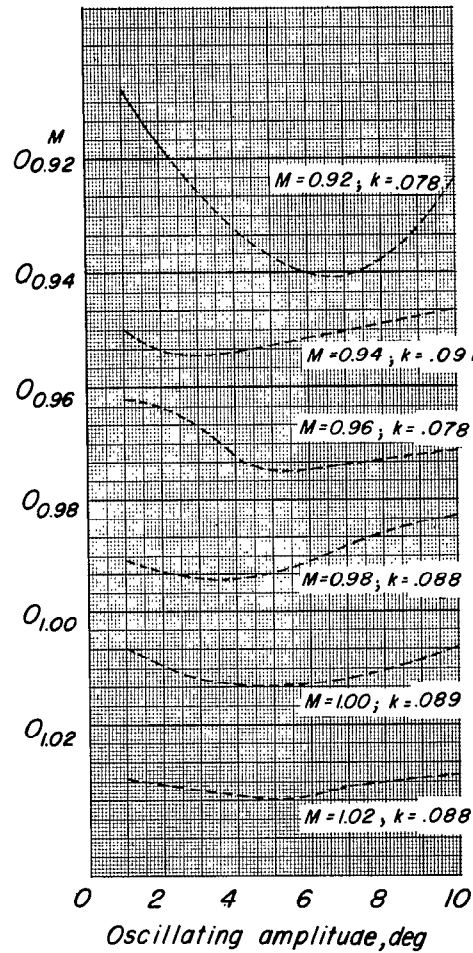
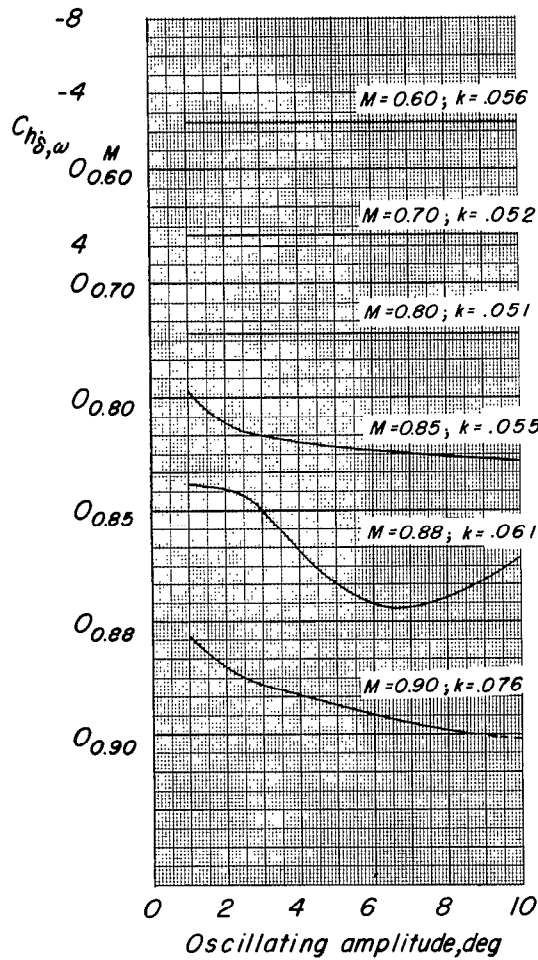
— Stable
 - - - Unstable

Flutter Characteristics

M	Flutter condition	Frequency cps	Amplitude deg
0.60	No flutter		
0.70			
0.80			
0.85			
0.88			
0.90			
0.91	↓		
0.92	B	200	9.0
0.96	S	217	13.9
0.98	S	213	14.9
1.00	S	217	15.1
1.02	S	214	14.9

(d) $f_0 = 110$.

Figure 10.- Continued.



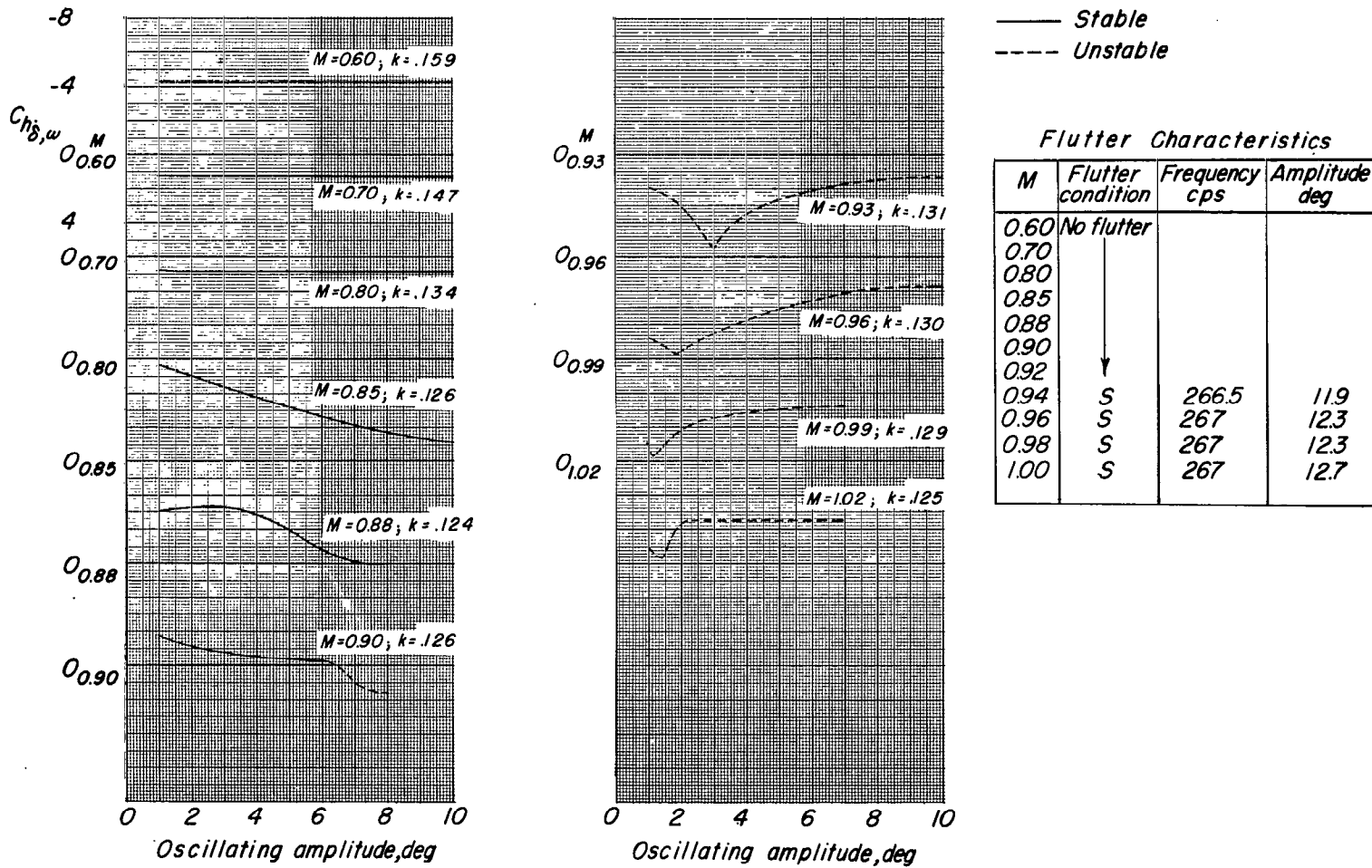
— Stable
 - - - Unstable

Flutter Characteristics

M	Flutter condition	Frequency cps	Amplitude deg
0.60	No flutter		
0.70			
0.80			
0.85			
0.88			
0.90			
0.91	B	165	11.9
0.94	S	176	14.0
1.02	S	180	15.2

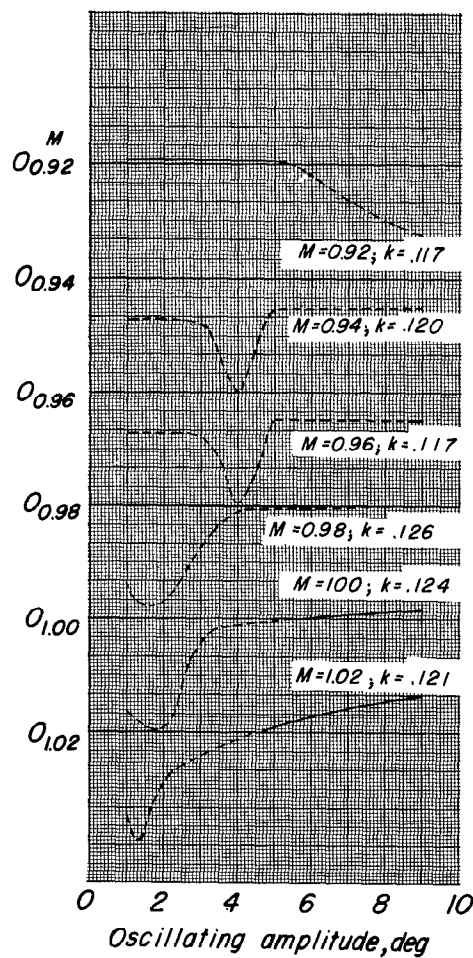
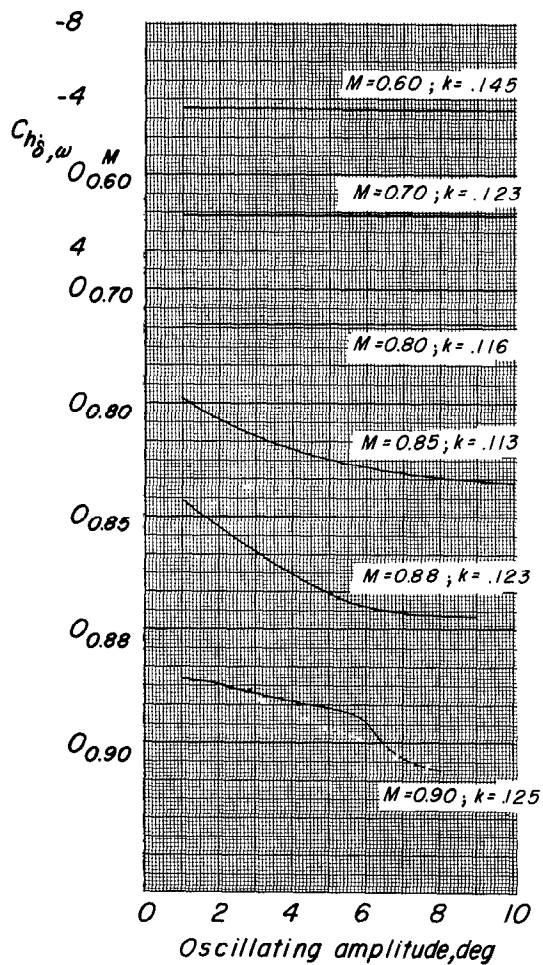
(e) $f_0 = 0$.

Figure 10.- Concluded.



(a) $f_0 = 202$.

Figure 11.- Flutter characteristics and variation of $C_{h\delta, \omega}$ with oscillating amplitude for various Mach numbers. $\alpha = 6^\circ$; $T = 0.17$.

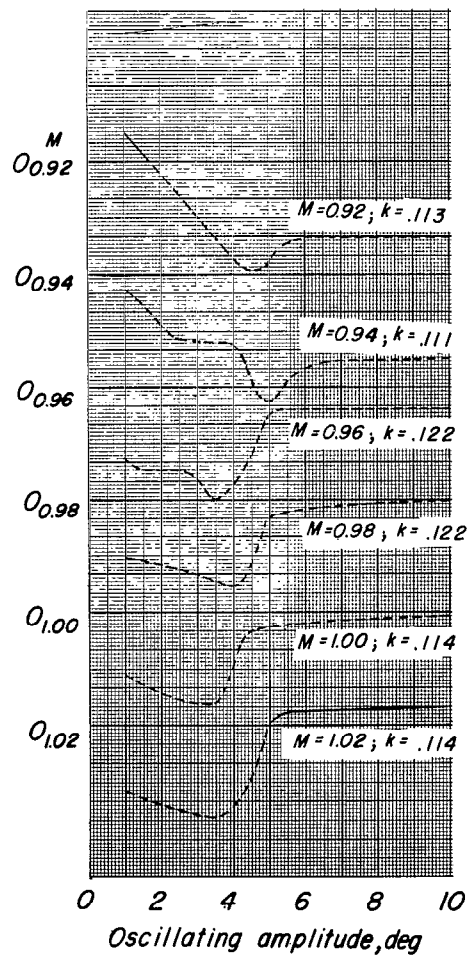
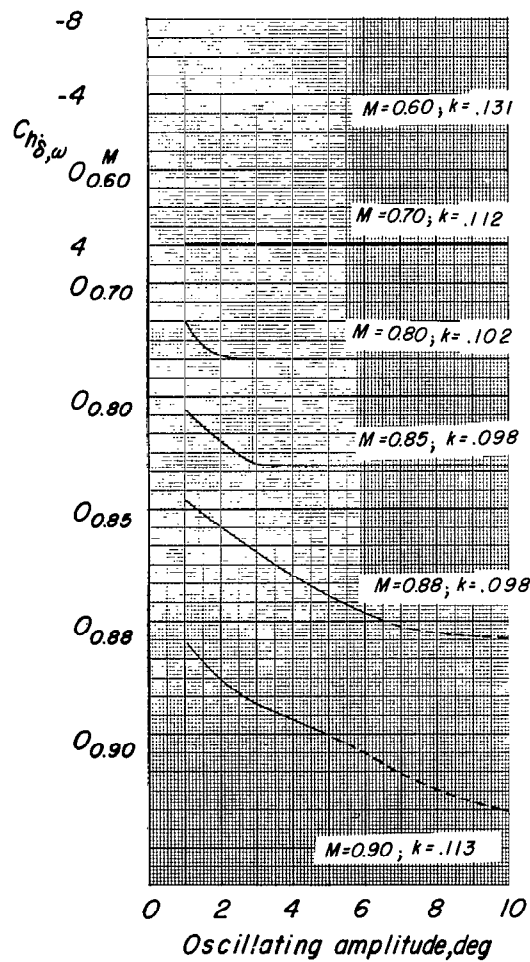


— Stable
 - - - Unstable

No flutter data obtained due to model failure.

(b) $f_0 = 170$.

Figure 11.- Continued.

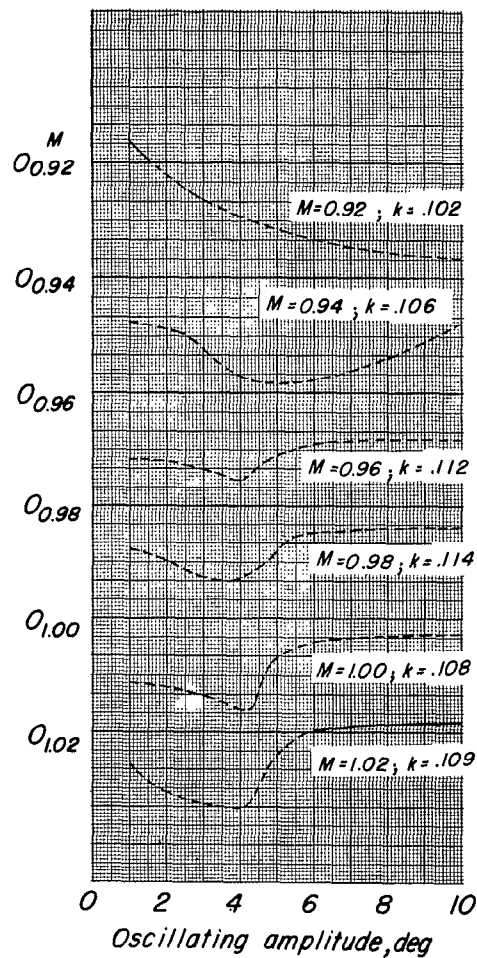
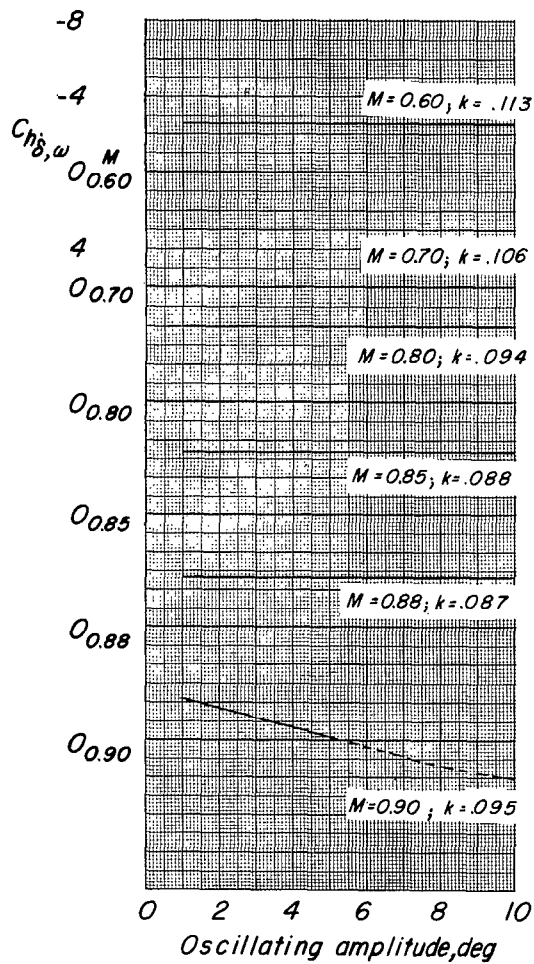


— Stable
 - - - Unstable

No flutter data obtained due to model failure.

(c) $f_0 = 138$.

Figure 11.- Continued.

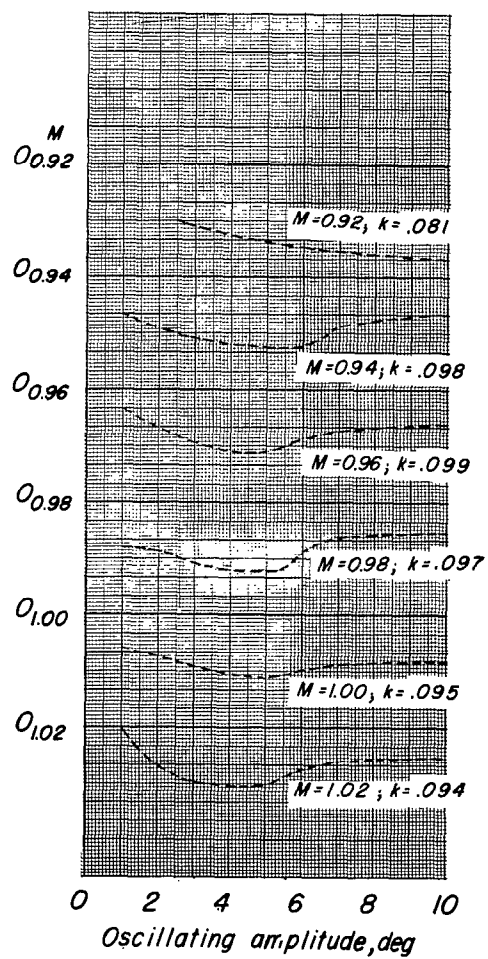
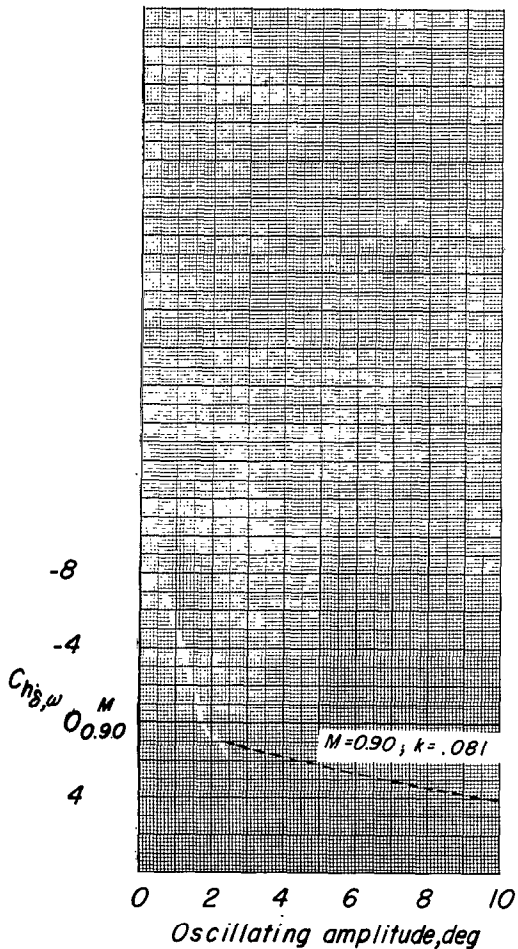


— Stable
 - - - Unstable

No flutter data obtained
 due to model failure

(d) $f_0 = 110$.

Figure 11.- Continued.

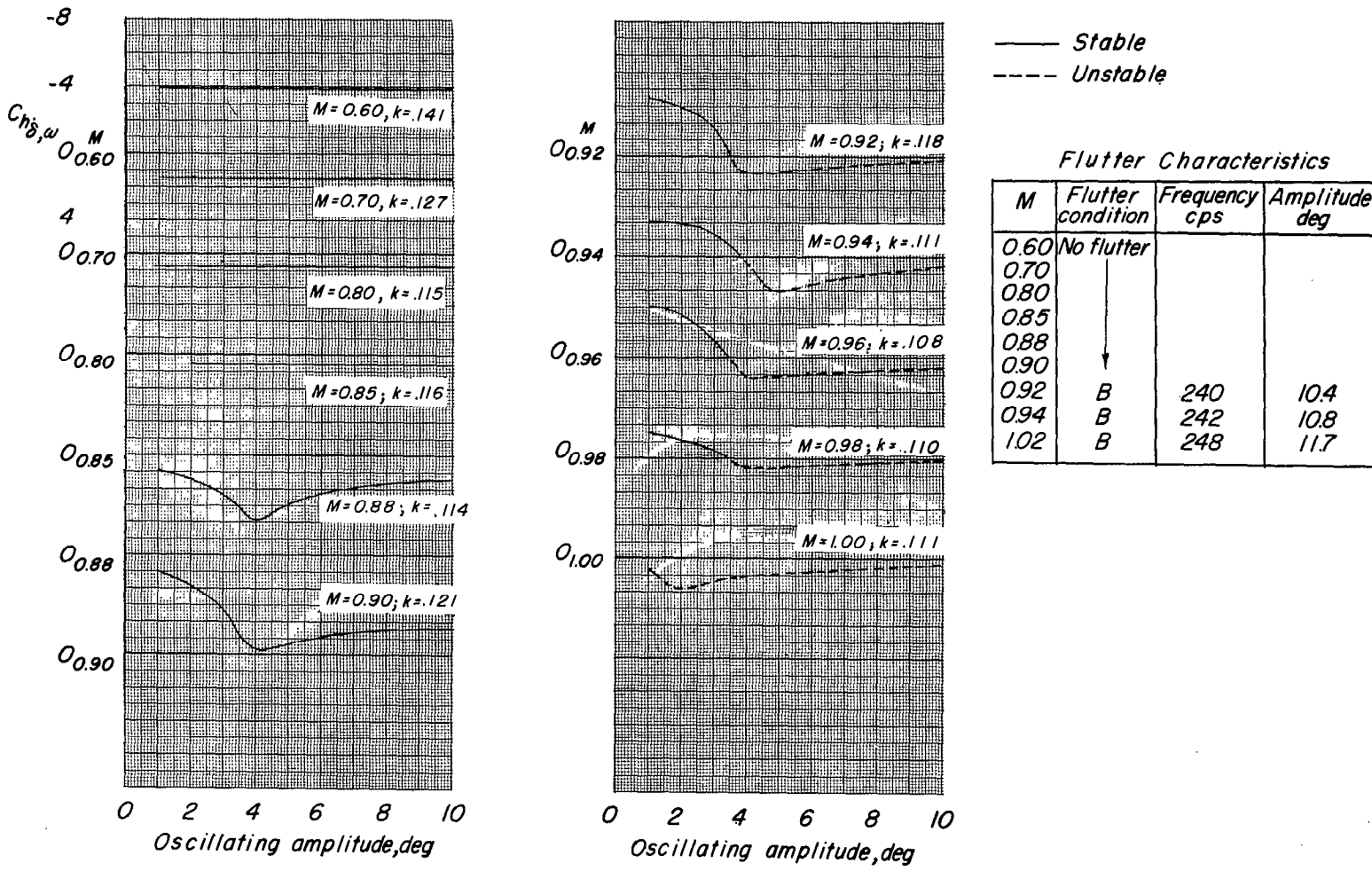


— Stable
 - - - Unstable

No flutter data obtained due to model failure.

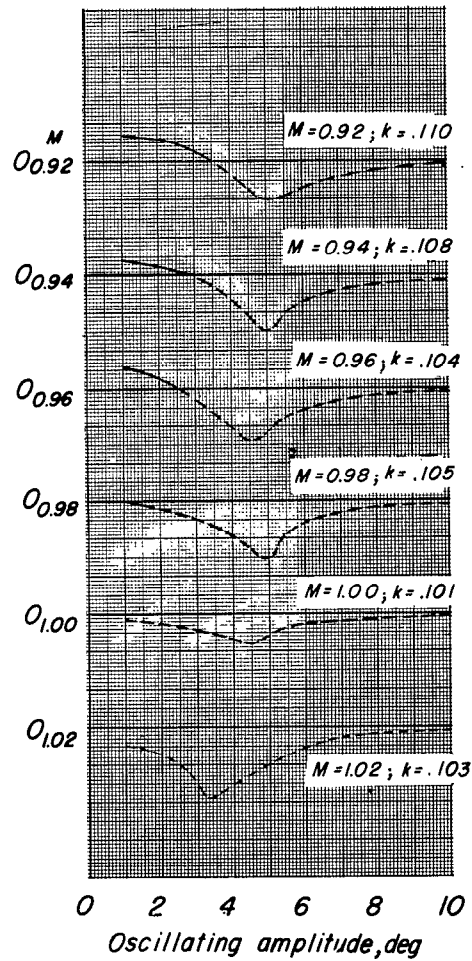
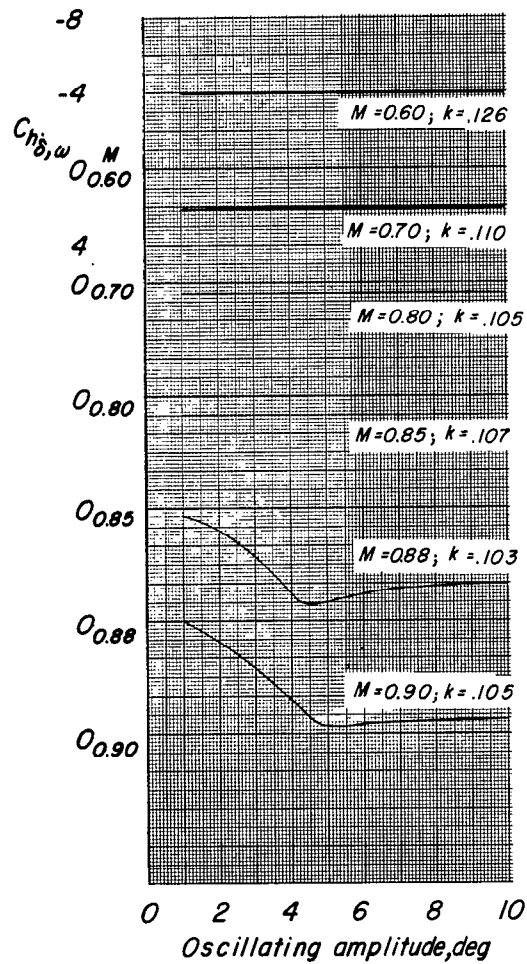
(e) $f_0 = 0.$

Figure 11.- Concluded.



(a) $f_o = 167$.

Figure 12.- Flutter characteristics and variation of $C_{h\delta, \omega}$ with oscillating amplitude for various Mach numbers. $\alpha = 0^\circ$; $T = 1.00$.



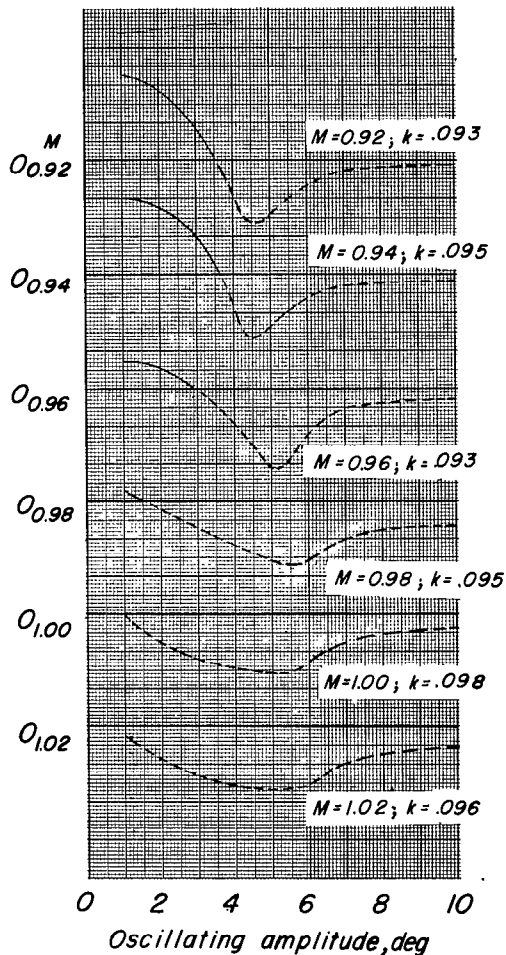
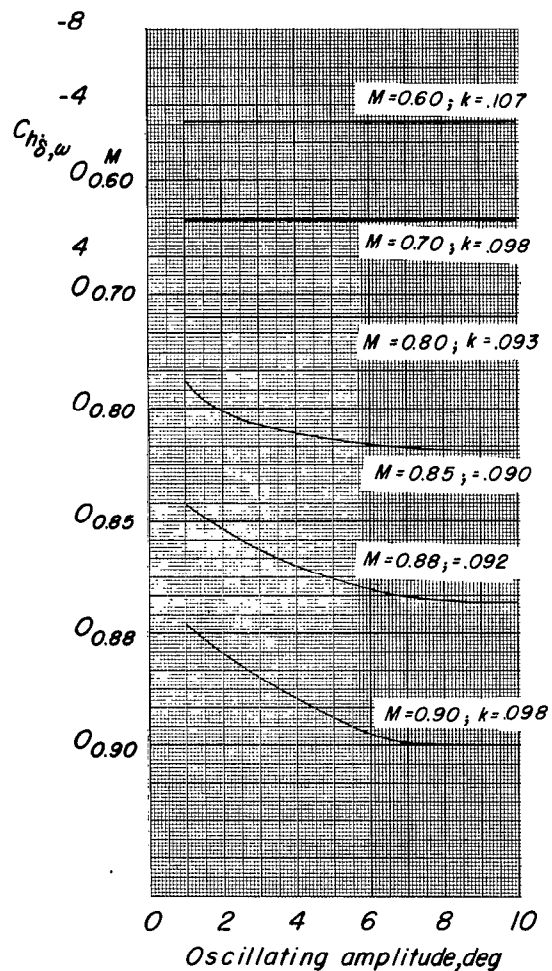
— Stable
 - - - Unstable

Flutter Characteristics

M	Flutter condition	Frequency cps	Amplitude deg
0.60	No flutter		
0.70			
0.80			
0.85			
0.88			
0.90			
0.91	B	223	10.7
1.02	S	233	13.4

(b) $f_0 = 144$.

Figure 12.- Continued.



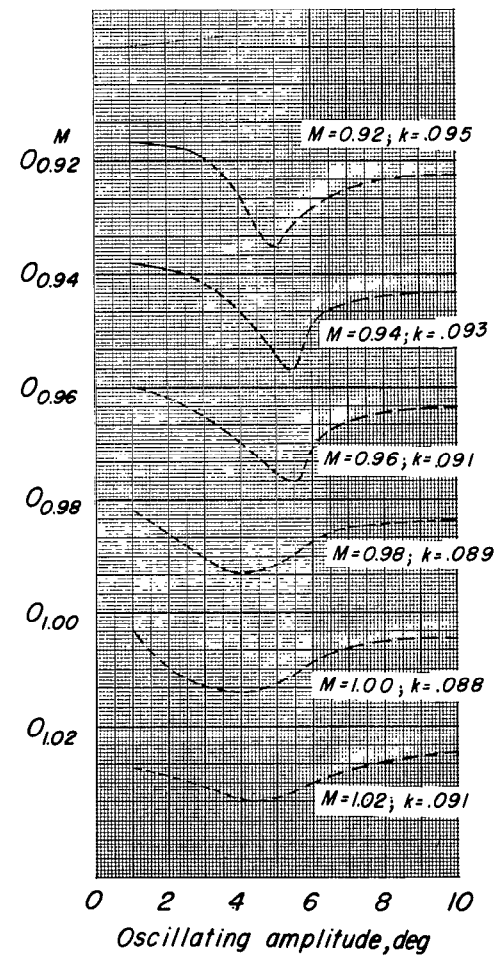
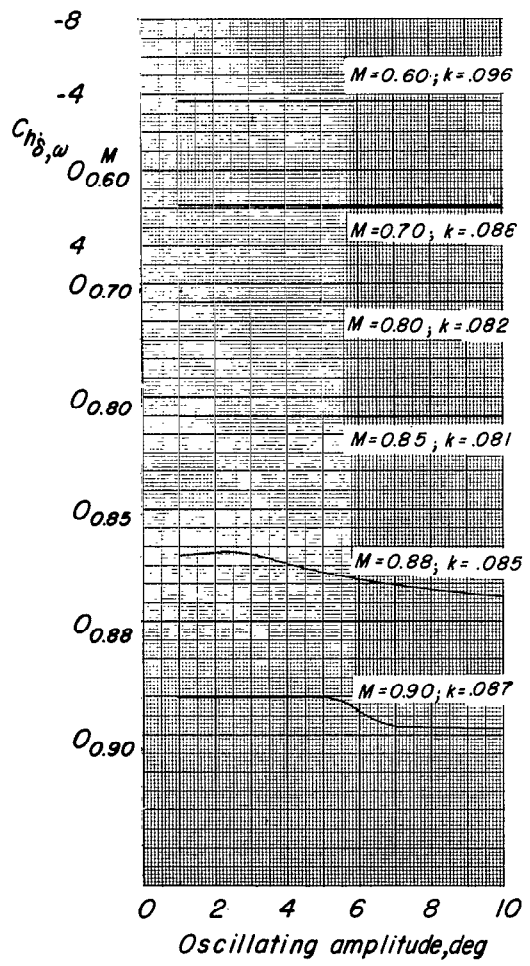
— Stable
 - - - Unstable

Flutter Characteristics

M	Flutter condition	Frequency cps	Amplitude deg
0.60	No flutter		
0.70	↓		
0.80			
0.85			
0.88			
0.90	B	213	12.5
1.00	S	217	13.8
1.02	S	220	14.0

(c) $f_0 = 121$.

Figure 12.- Continued.



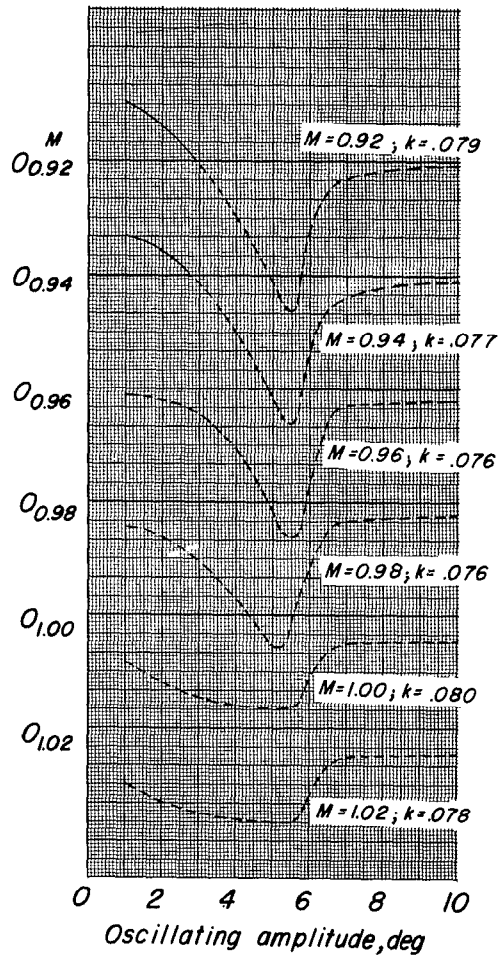
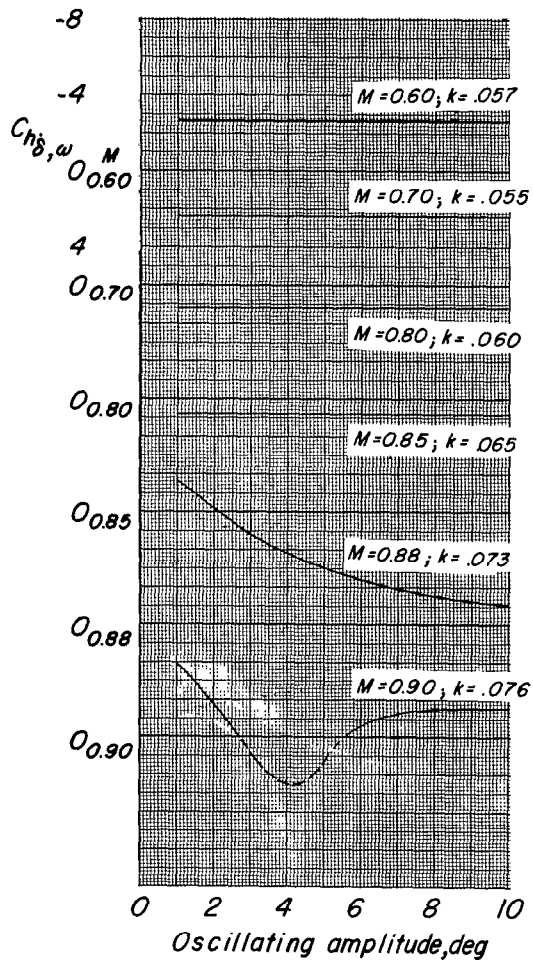
— Stable
 - - - Unstable

Flutter Characteristics

M	Flutter condition	Frequency cps	Amplitude deg
0.60	No flutter		
0.70			
0.80			
0.85			
0.88			
0.90			
0.92	B	194	11.6
0.96	S	195	12.5
0.98	S	198	13.6
1.00	S	199	13.8
1.02	S	200	13.7

(a) $f_0 = 96$.

Figure 12.- Continued.



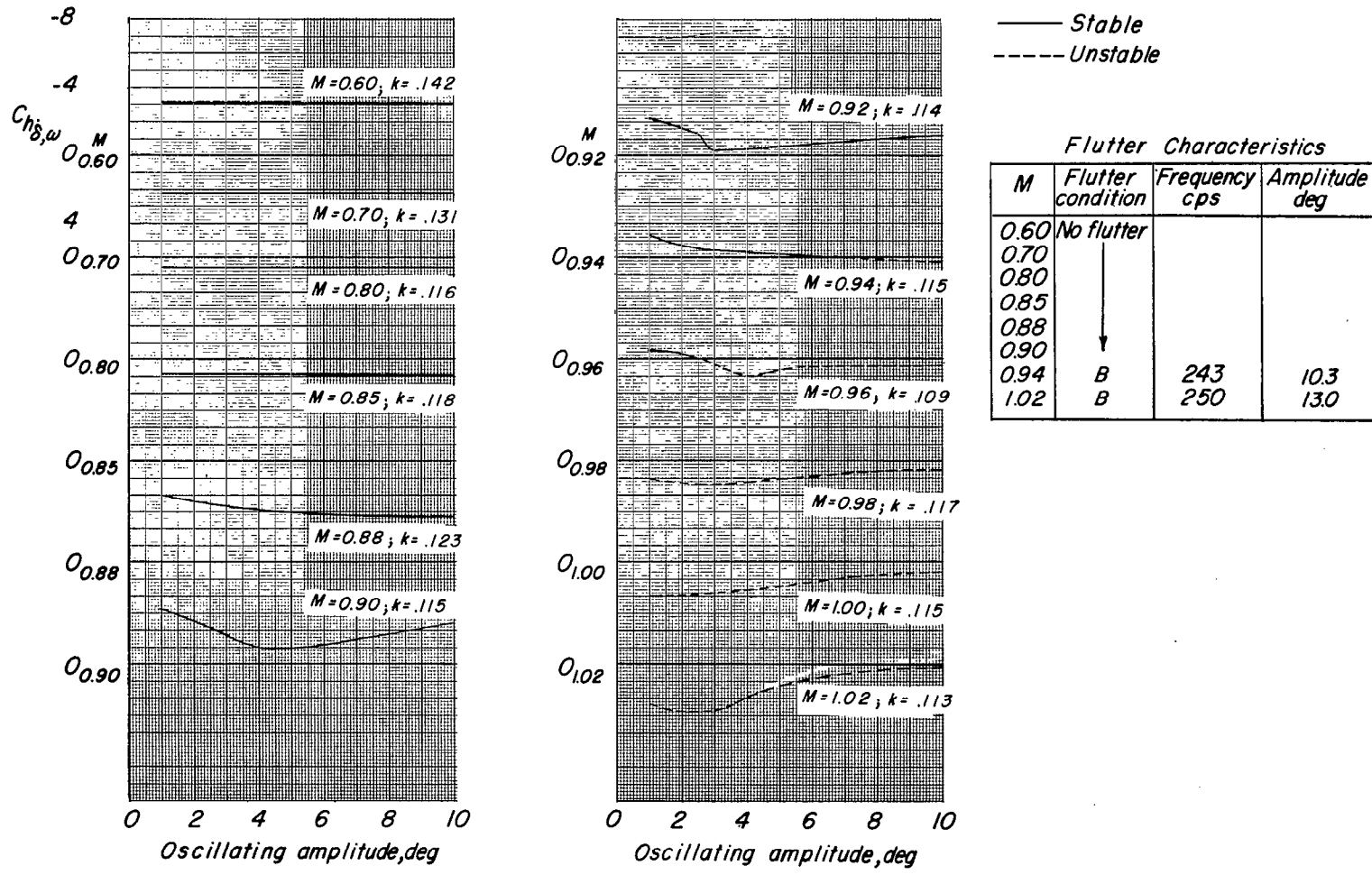
— Stable
 - - - Unstable

Flutter Characteristics

M	Flutter condition	Frequency cps	Amplitude deg
0.60	No flutter		
0.70			
0.80			
0.85			
0.88			
0.90			
0.92	B	167	12.4
0.96	S	175	13.7
0.98	S	178	14.6
1.00	S	175	14.0
1.02	S	177	14.5

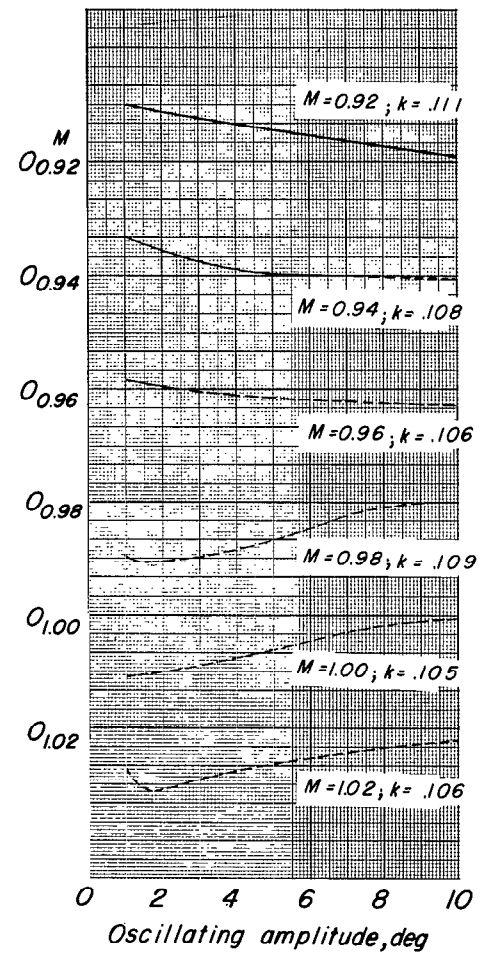
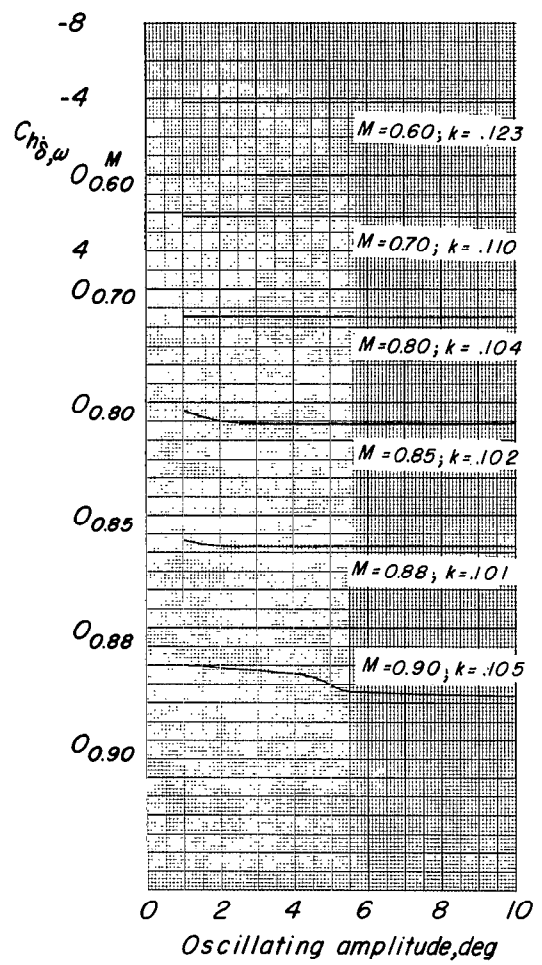
(e) $f_0 = 0$.

Figure 12.- Concluded.



(a) $f_0 = 167$.

Figure 13.- Flutter characteristics and variation of $C_{h\delta, \omega}$ with oscillating amplitude for various Mach numbers. $\alpha = 6^\circ$; $T = 1.00$.



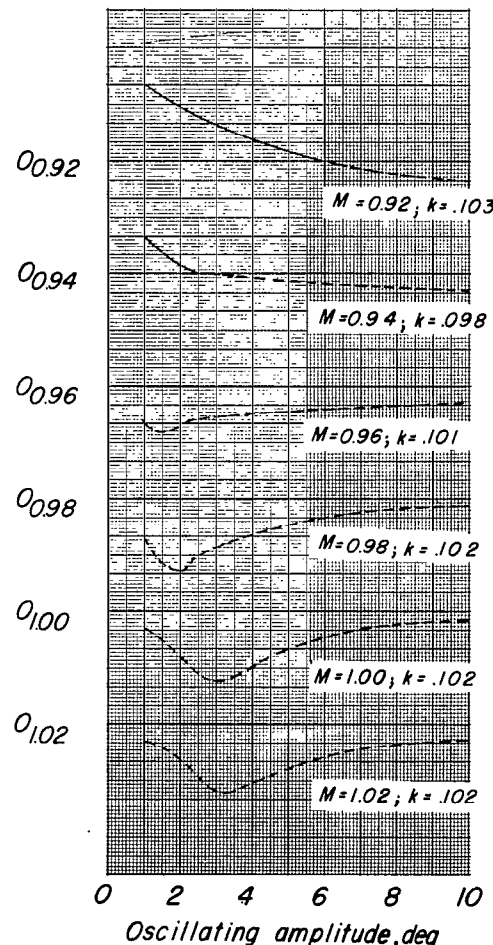
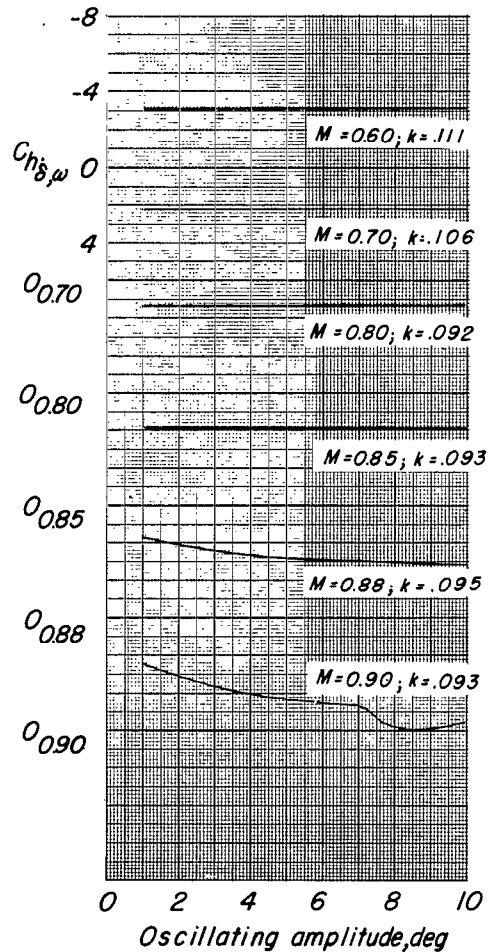
— Stable
 - - - Unstable

Flutter Characteristics

M	Flutter condition	Frequency cps	Amplitude deg
0.60	No flutter		
0.70			
0.80			
0.85			
0.88			
0.90	B	226	13.5
0.92			
1.02			

(b) $f_0 = 144$.

Figure 13.- Continued.



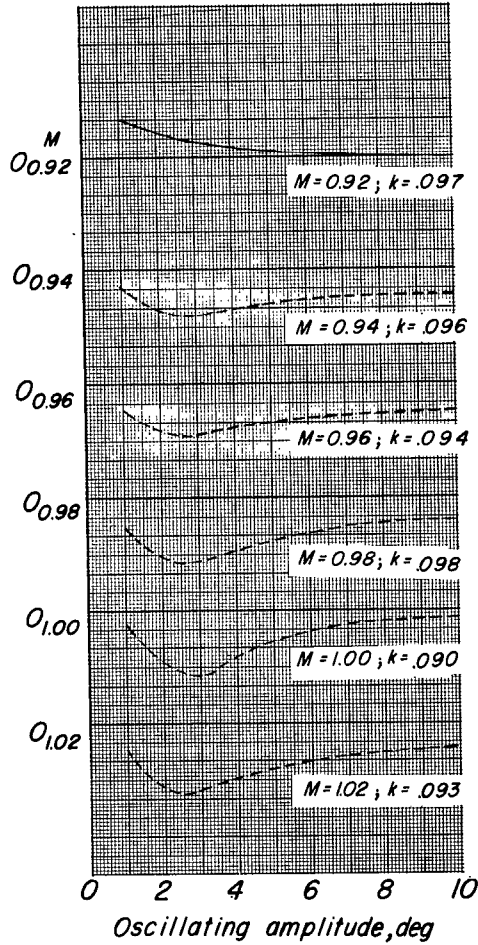
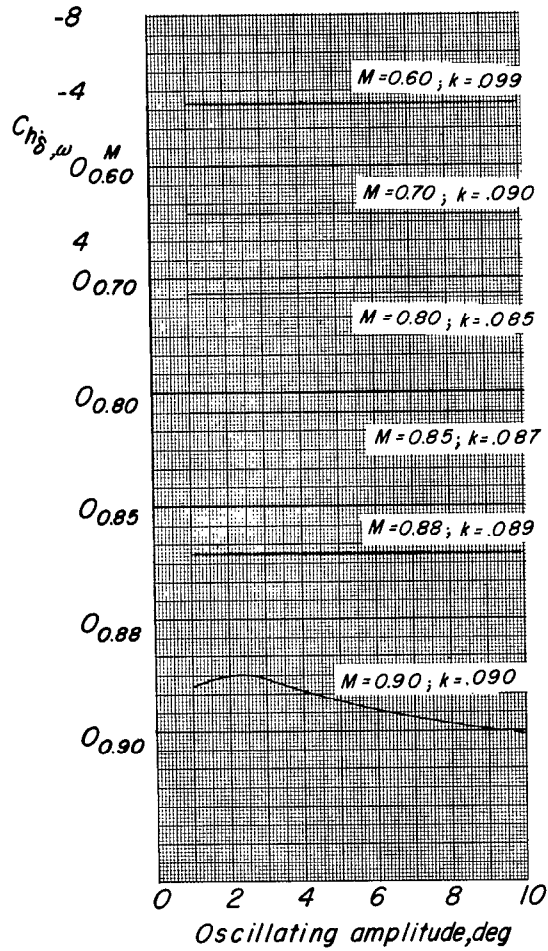
— Stable
 - - - Unstable

Flutter Characteristics

M	Flutter condition	Frequency cps	Amplitude deg
0.60	No flutter		
0.70			
0.80			
0.85			
0.88			
0.90			
0.92	B	214	137
0.94	B	214	137
0.96	S	2165	144
0.98	S	222	154
1.00	S	222	15.2
1.02	S	222	15.0

(c) $f_0 = 121$.

Figure 13.- Continued.



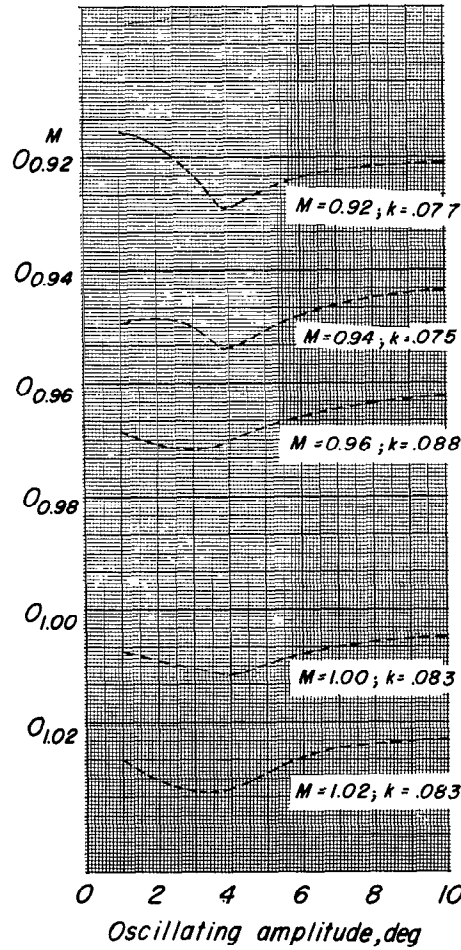
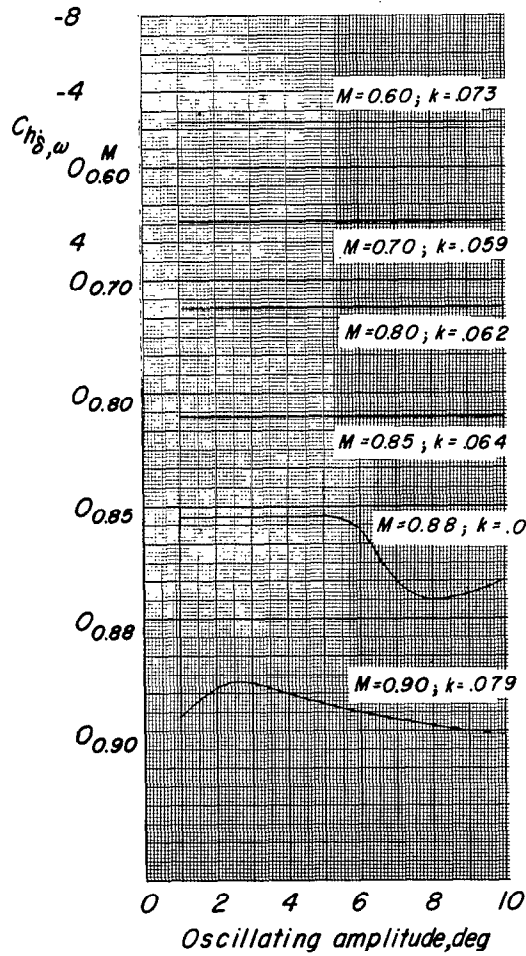
— Stable
 - - - Unstable

Flutter Characteristics

M	Flutter condition	Frequency cps	Amplitude deg
0.60	No flutter		
0.70			
0.80			
0.85			
0.88			
0.90			
0.92	B	196	13.7
0.94	S	196	14.1
0.96	S	205	15.0
0.98	S	205	15.5
1.00	S	206	15.4
1.02	S	207	15.2

(d) $f_0 = 96$.

Figure 13.- Continued.



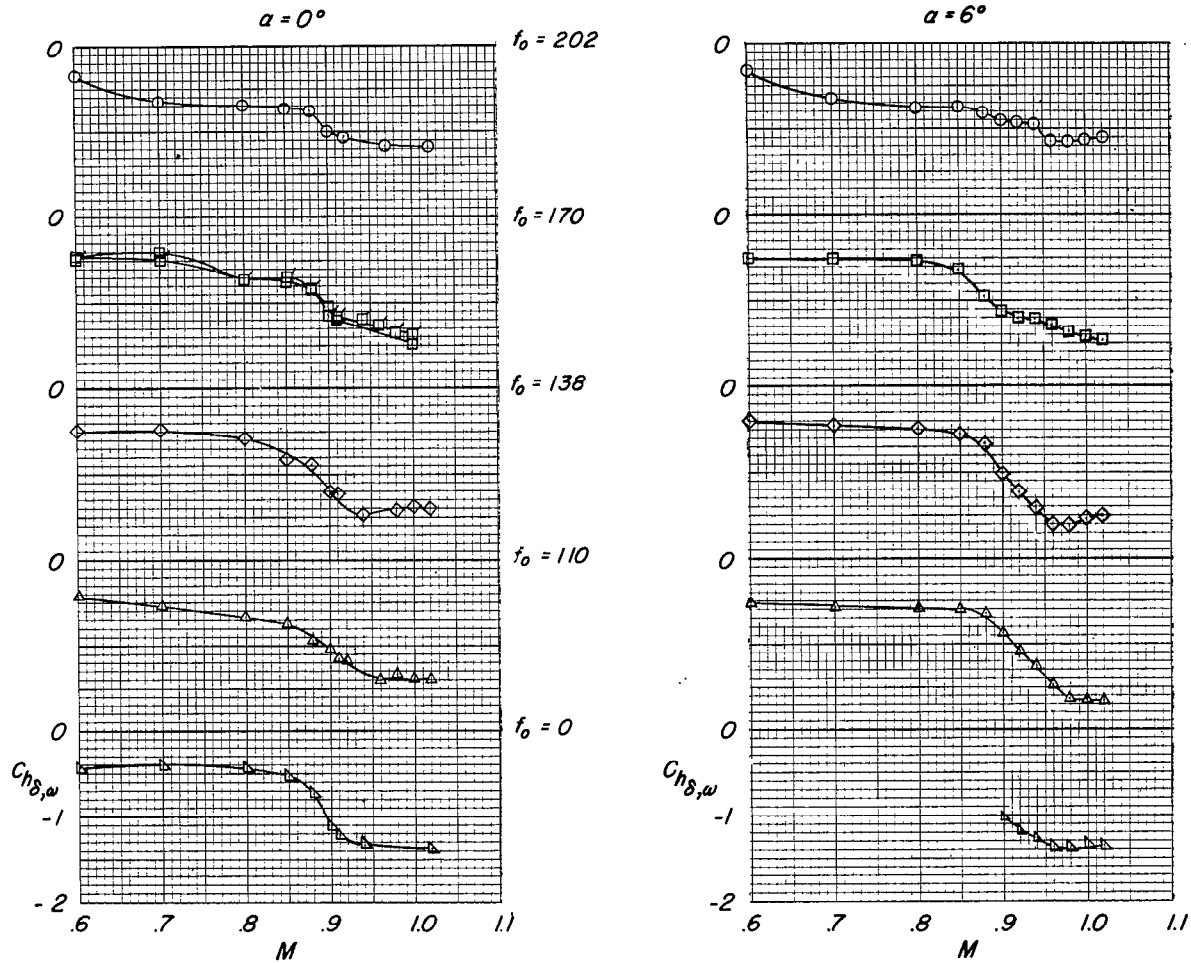
— Stable
 - - - Unstable

Flutter Characteristics

M	Flutter condition	Frequency cps	Amplitude deg
0.60	No flutter		
0.70			
0.80			
0.85			
0.88			
0.90	↓		
0.92	B	162	13.9
0.94	S	170	15.6
0.96	S	173.5	16.8
0.98	S	176	17.7
1.00	S	173.5	16.7
1.02	S	175	17.2

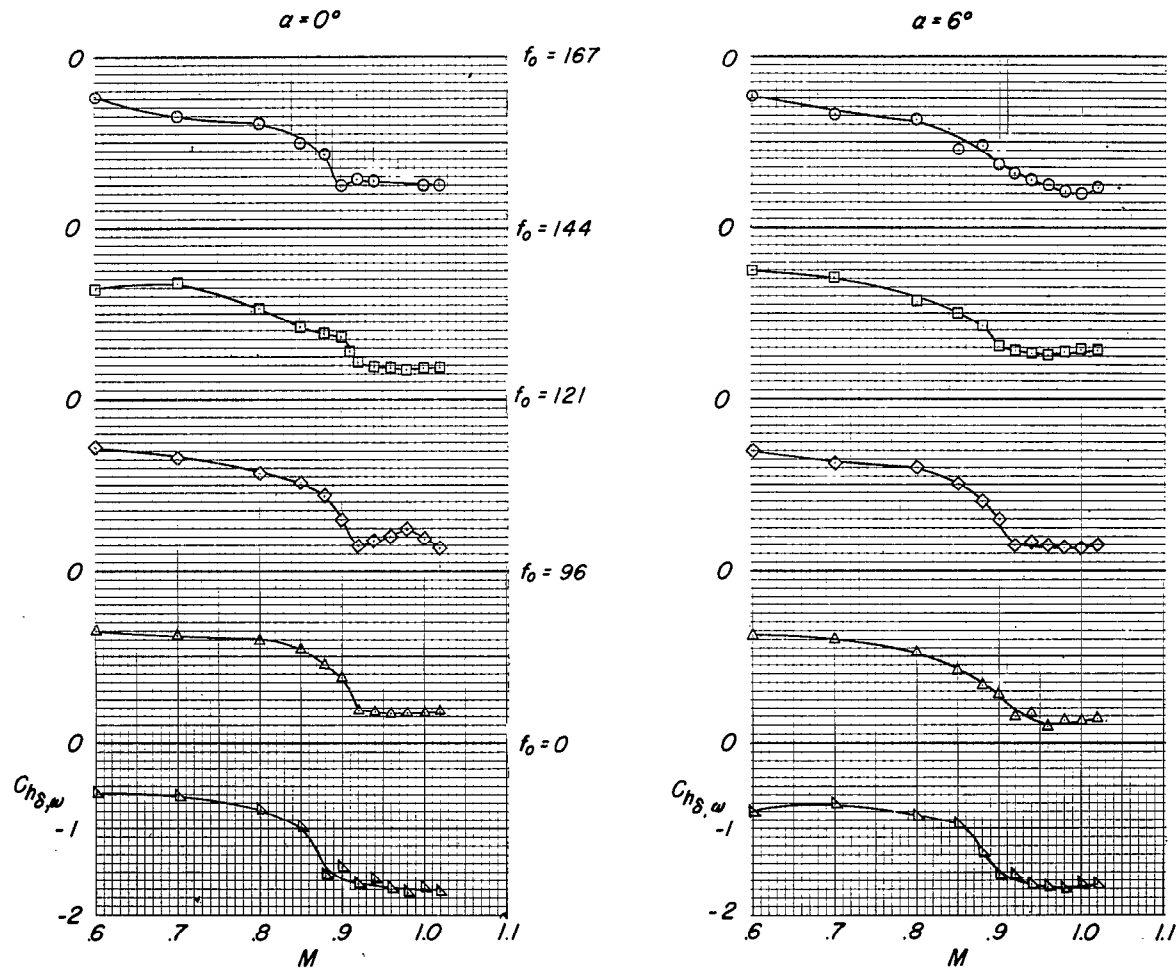
(e) $f_0 = 0$.

Figure 13.- Concluded.



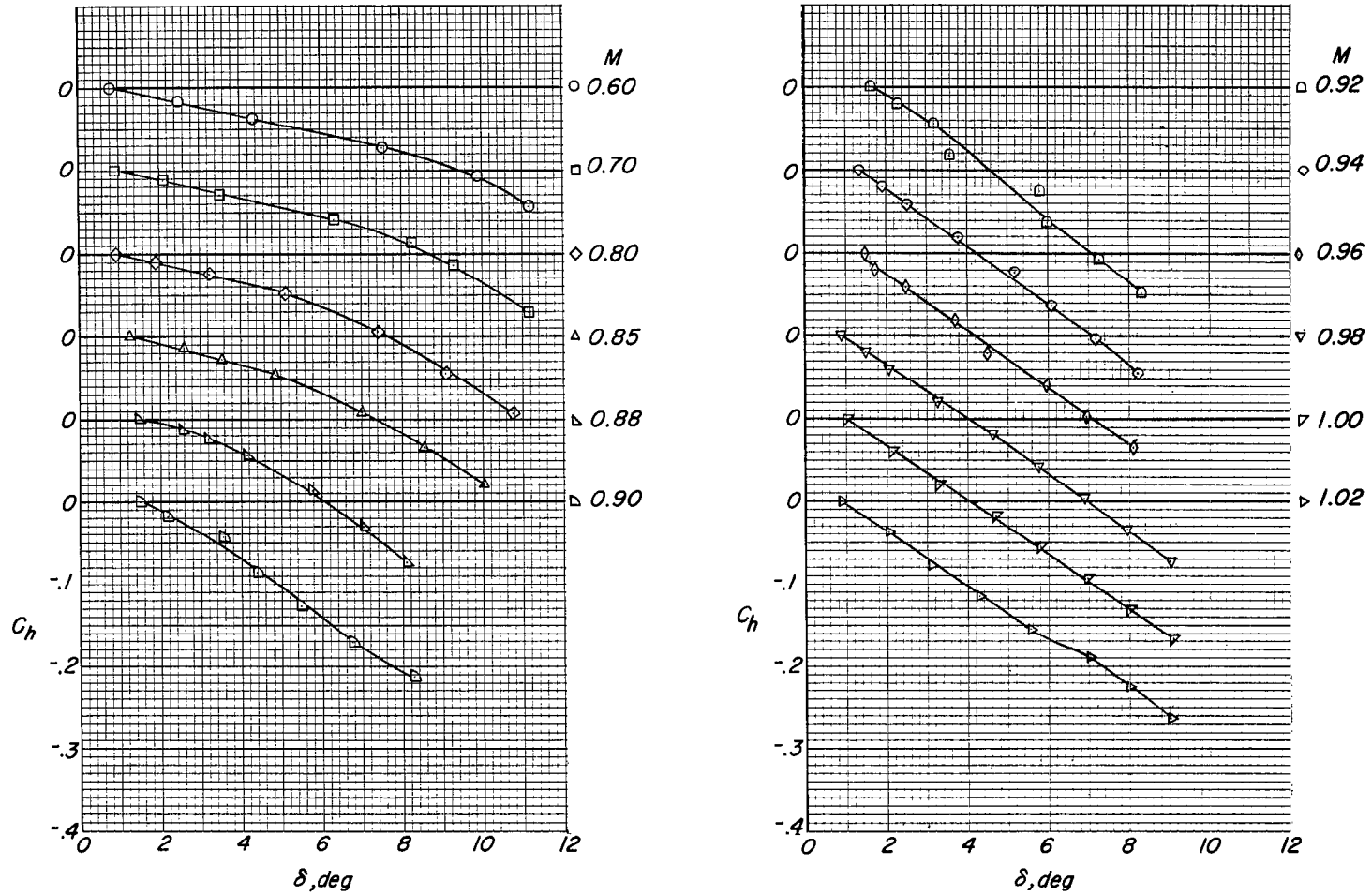
(a) $T = 0.17$.

Figure 14.- Variation of $C_{h\delta, \omega}$ with Mach number for various wind-off natural frequencies. Flagged symbols are with tip store.



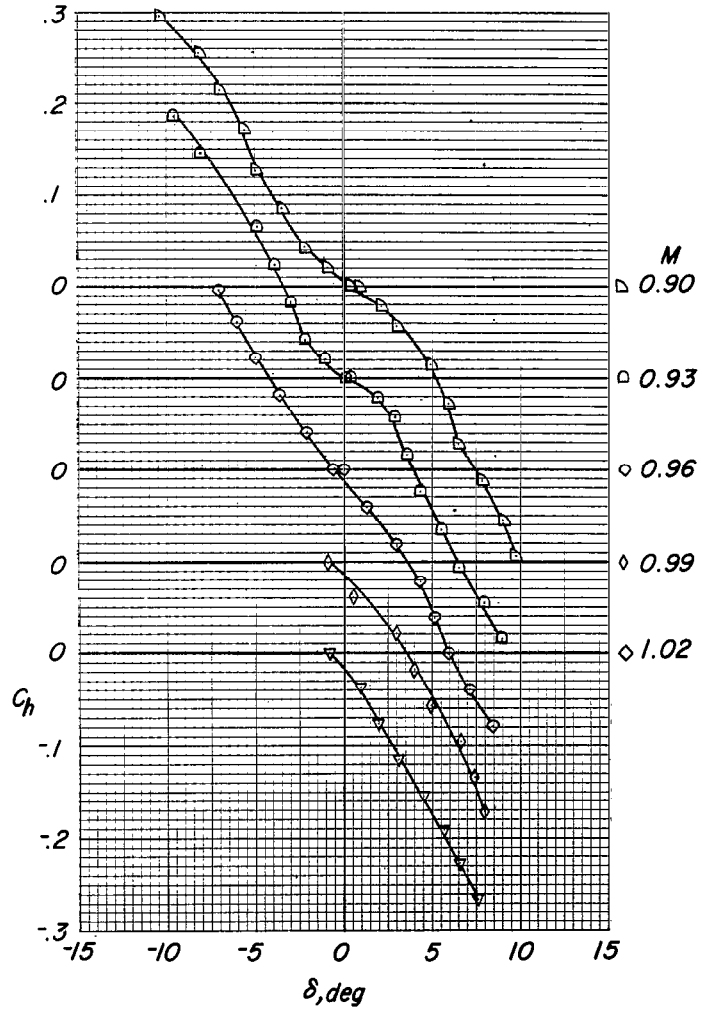
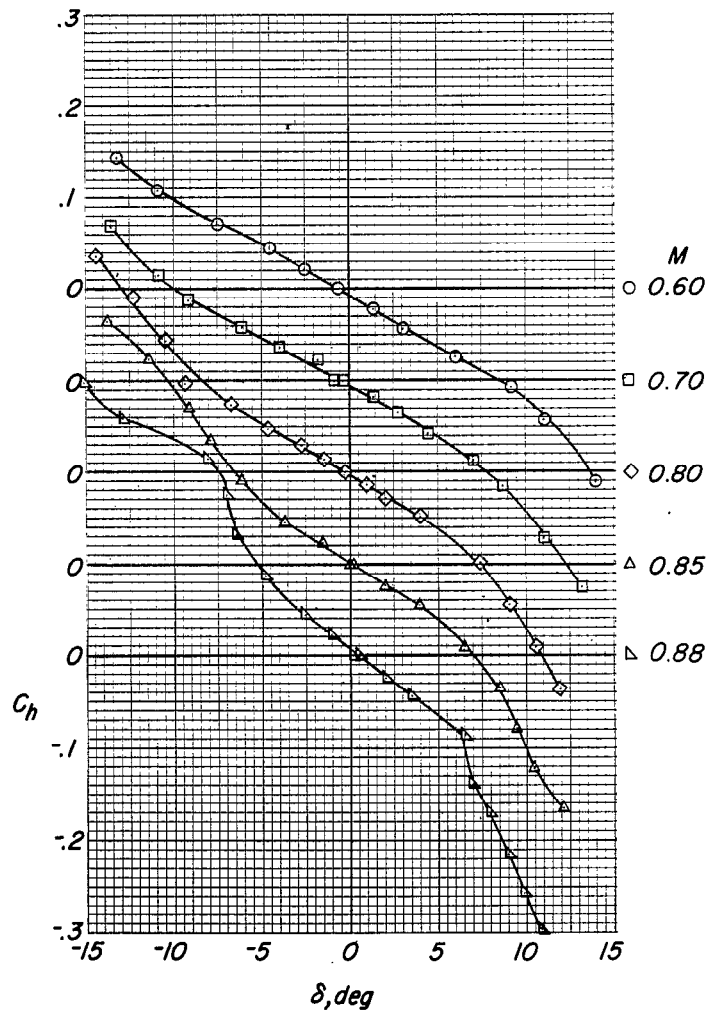
(b) $T = 1.0$.

Figure 14.- Concluded.



(a) $\alpha = 0^\circ$.

Figure 15.- Variation of static hinge-moment coefficient with control deflection for various Mach numbers. $T = 1.0$.



(b) $\alpha = 6^\circ$.

Figure 15.- Concluded.

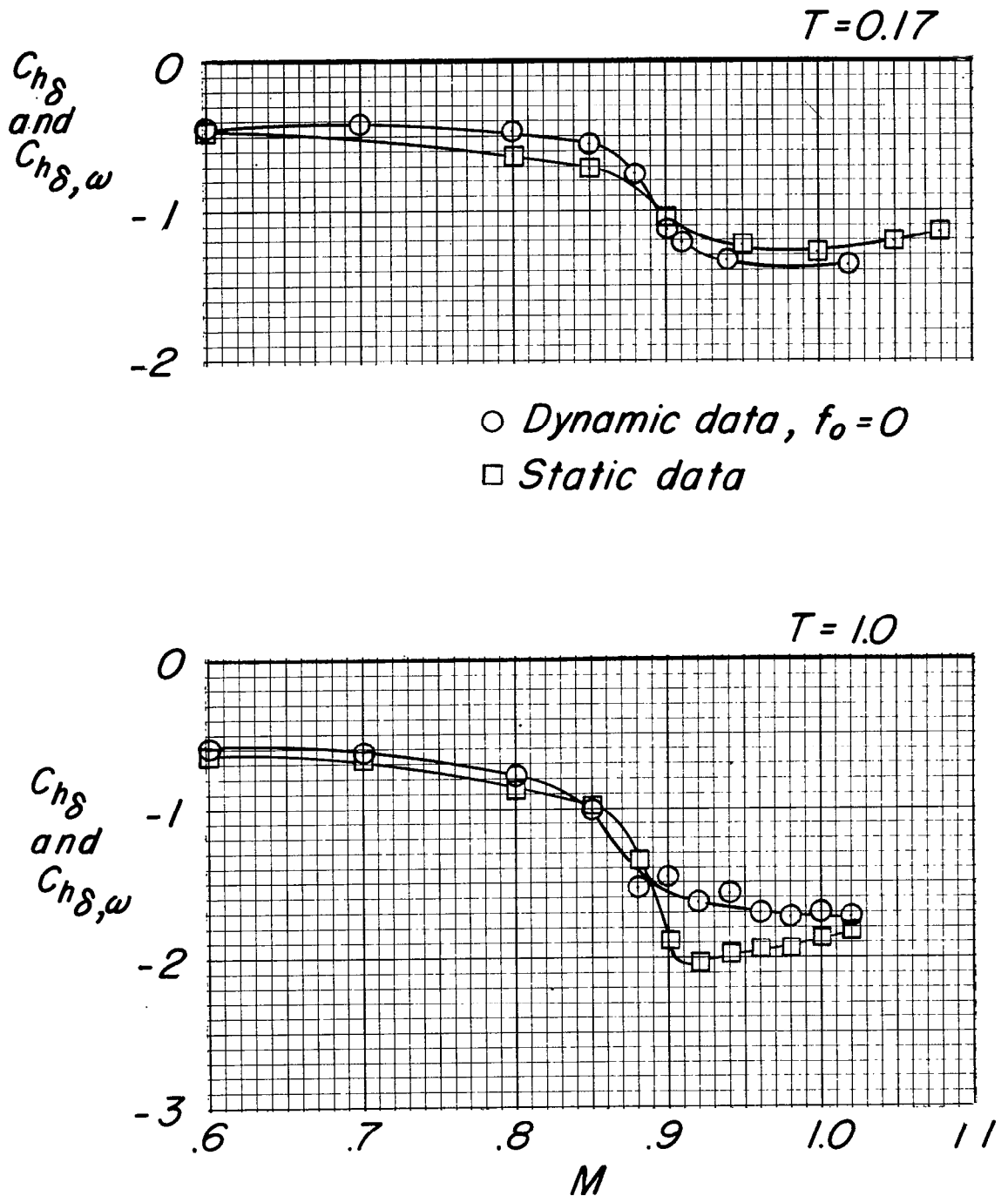


Figure 16.- Comparison of $C_{h\delta}$ as determined from static and dynamic tests at transonic Mach numbers. $\alpha = 0^\circ$.

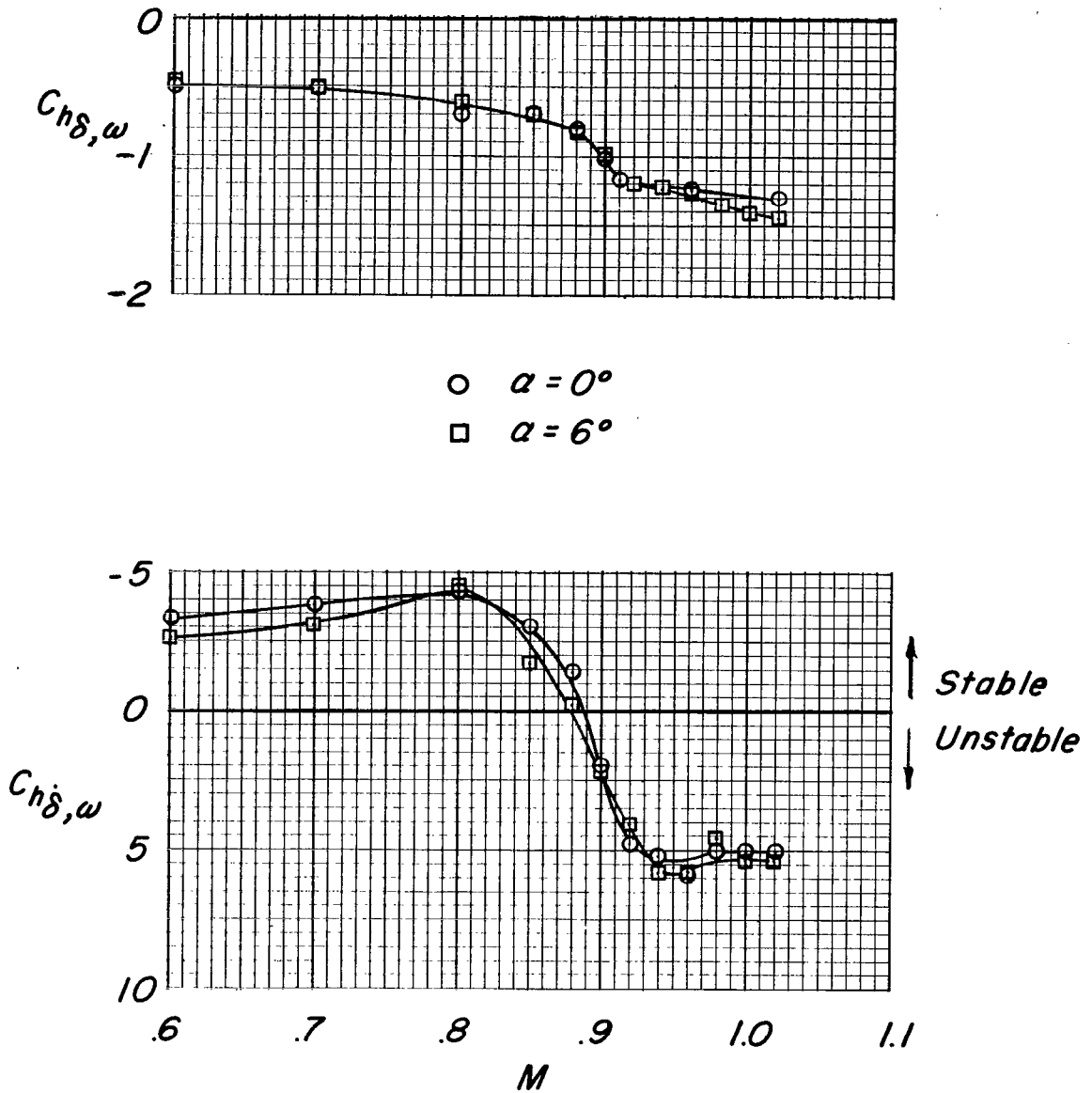


Figure 17.- Effect of angle of attack on the variation of $C_{h\delta, \omega}$ and $C_{h\dot{\delta}, \omega}$ with Mach number. $T = 0.17$; $k \approx 0.12$. (Maximum values of $C_{h\dot{\delta}, \omega}$ presented.)

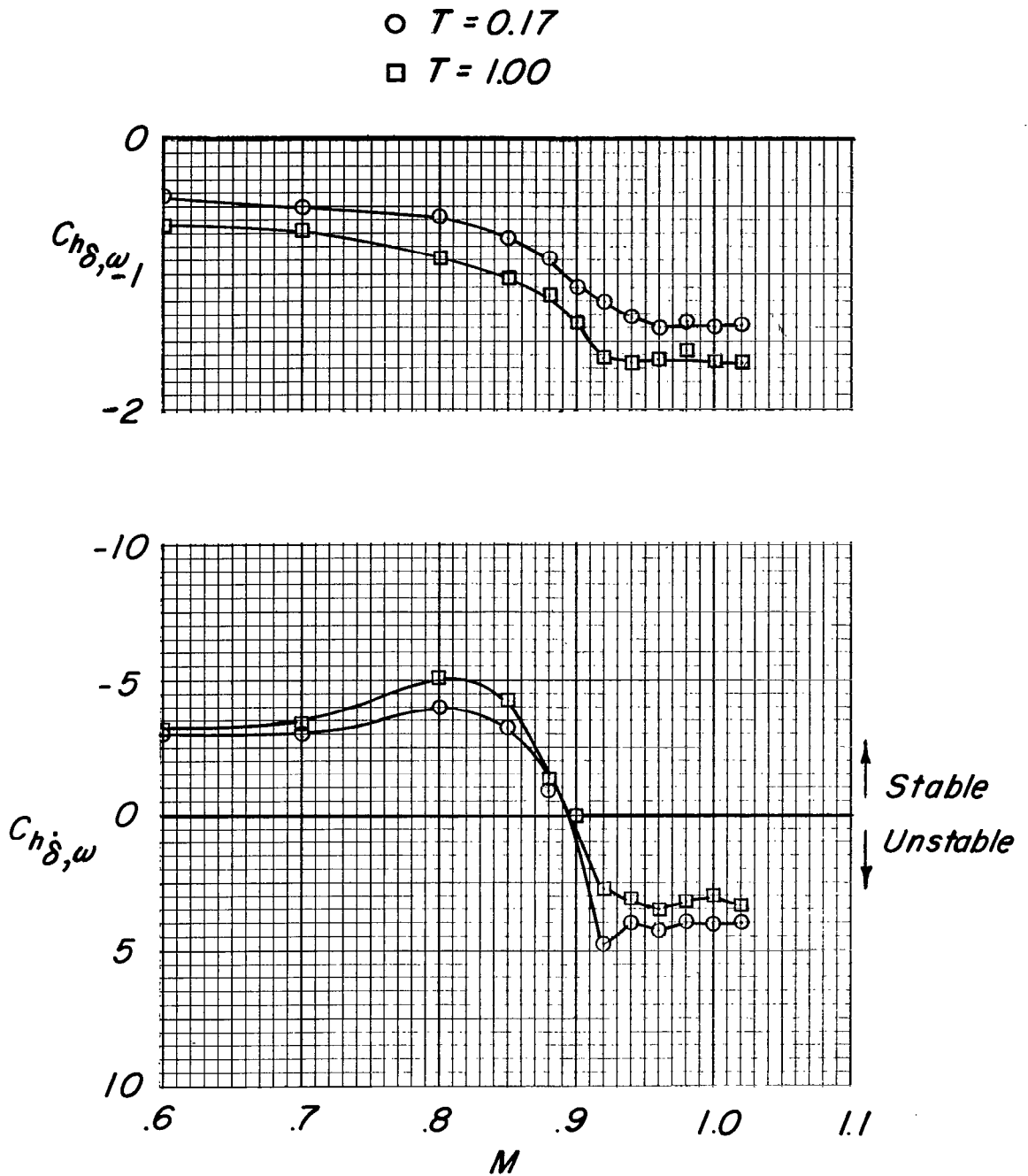


Figure 18.- Effect of trailing-edge thickness on $Ch_{\delta, \omega}$ and $Ch_{\delta, \omega}$ with Mach number. $\alpha = 0^\circ$; $k \approx 0.10$. (Maximum values of $Ch_{\delta, \omega}$ presented.)

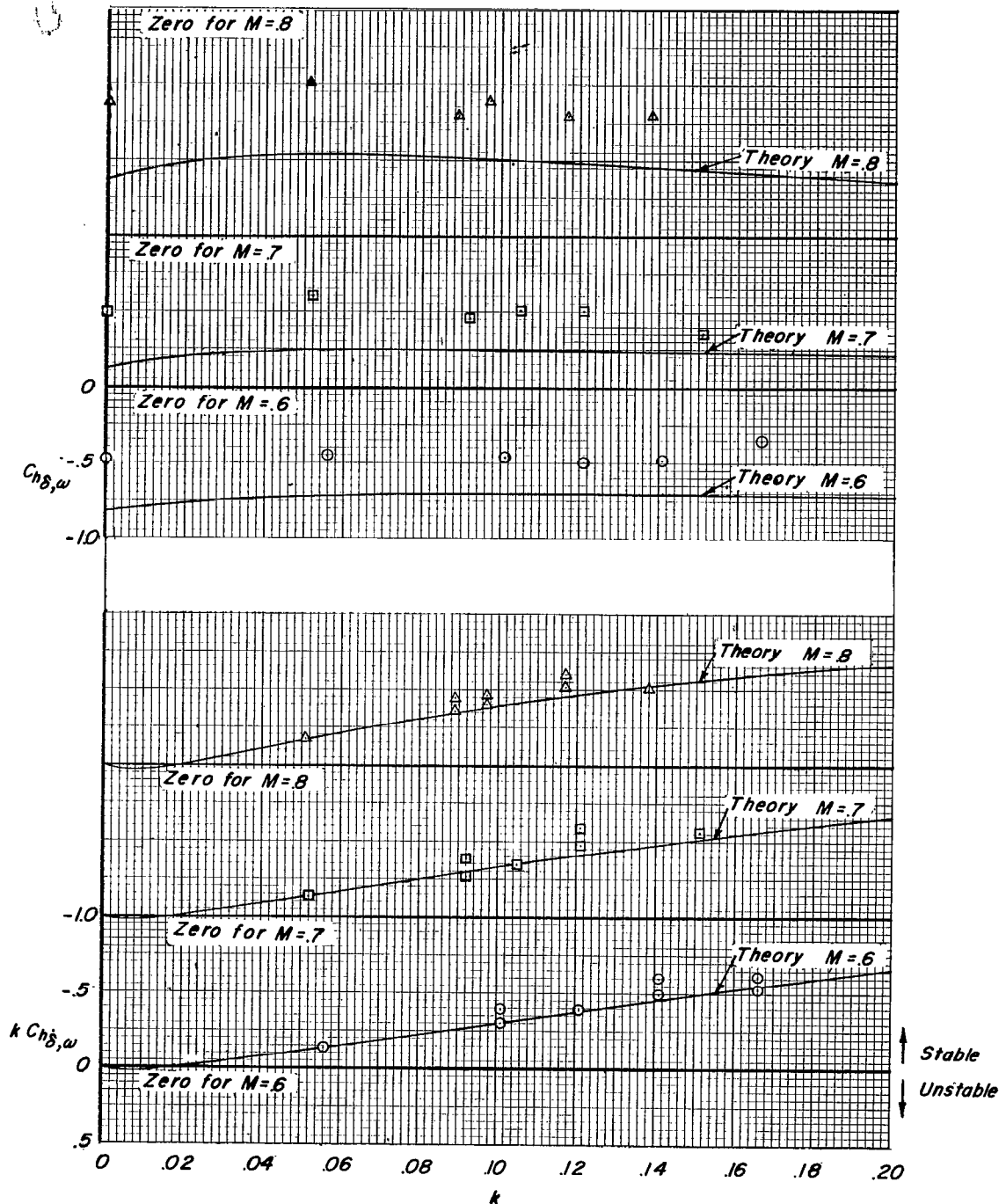


Figure 19.- Comparison of experimental oscillating hinge-moment coefficients with the subsonic theory of reference 10. (Theory has been modified by an experimental correction to account for aerodynamic balance.) $\alpha = 0^\circ$; $T = 0.17$.

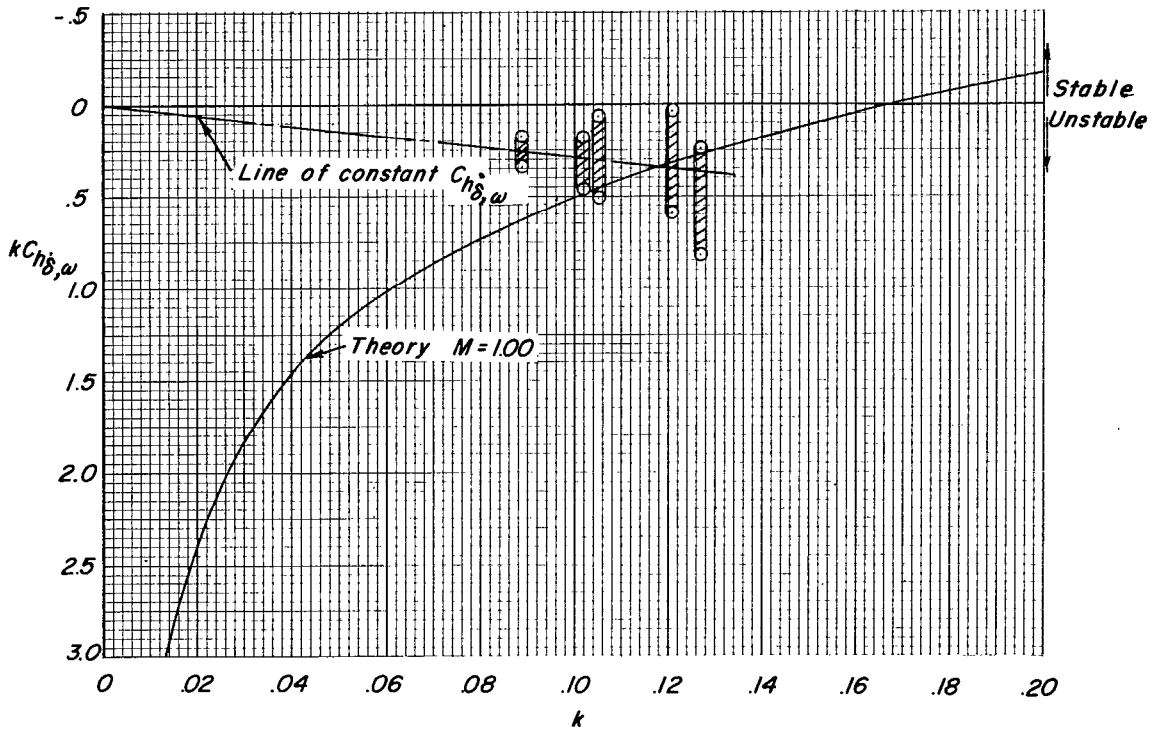
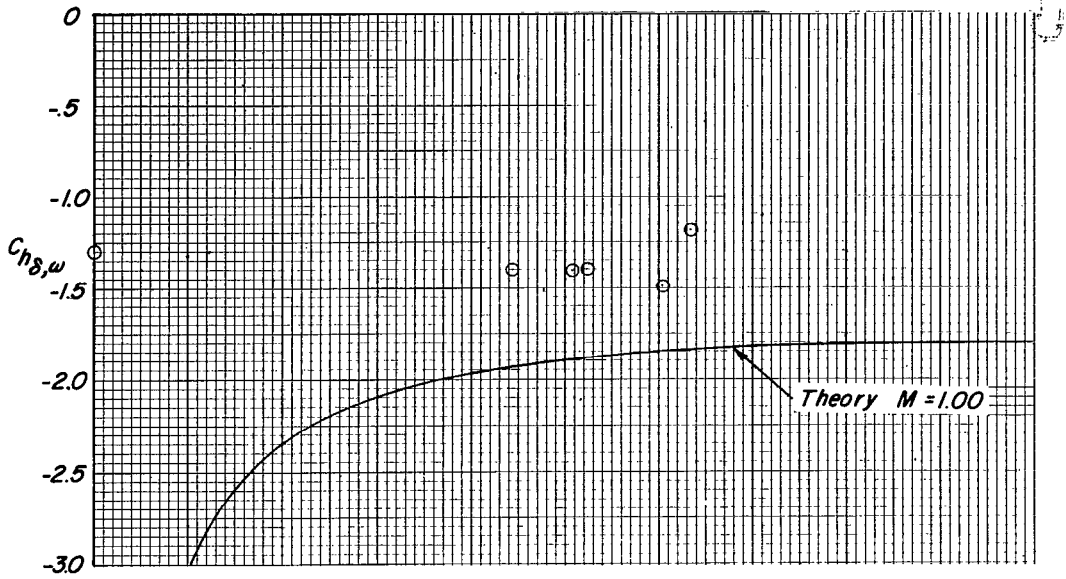


Figure 20.- Comparison of experimental oscillating hinge-moment coefficients with the sonic theory of reference 12.

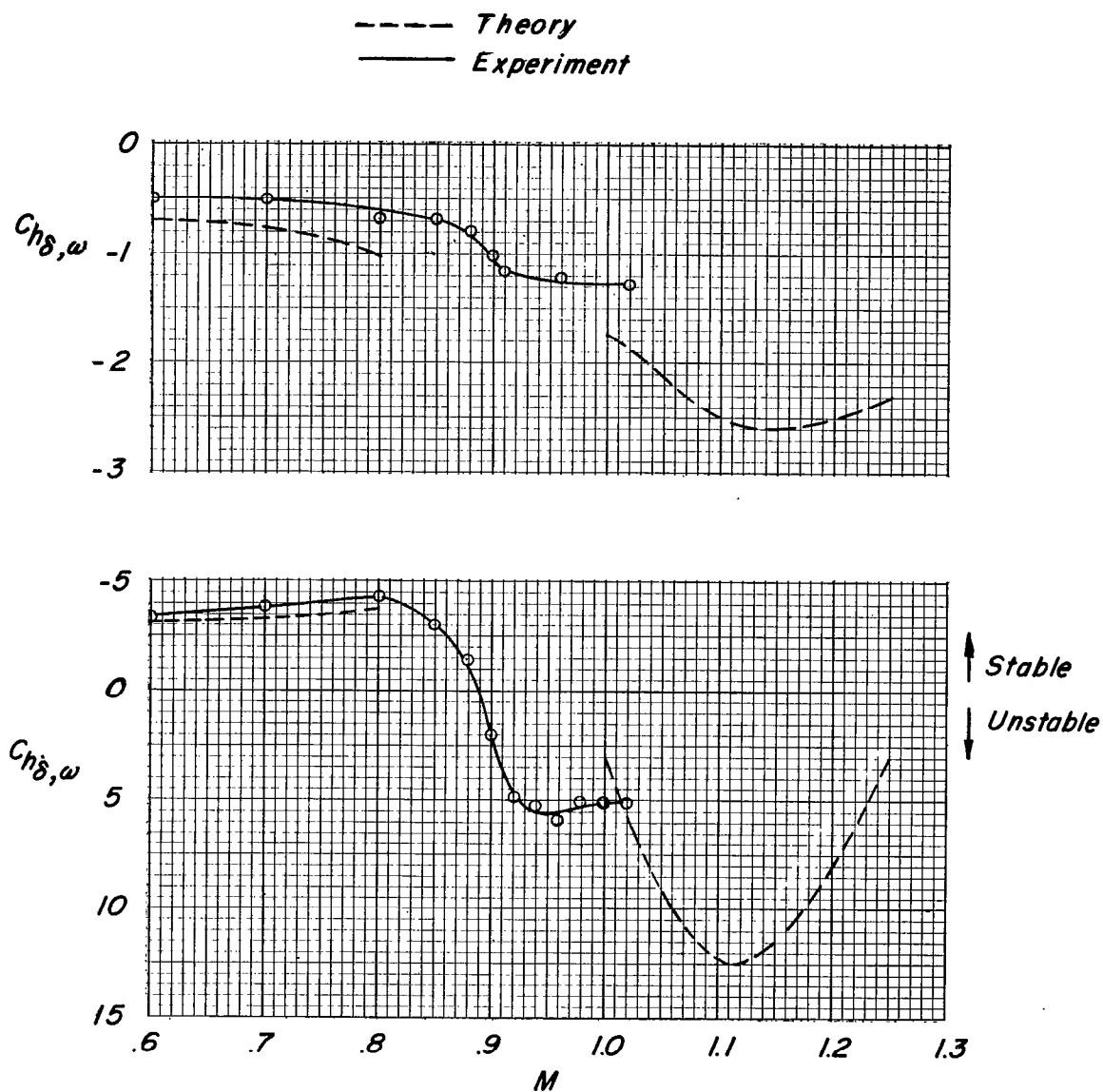


Figure 21.- Comparison of experimental oscillation hinge-moment coefficients with theory through the Mach number range. $k = 0.12$; $T = 0.17$; $\alpha = 0^\circ$.

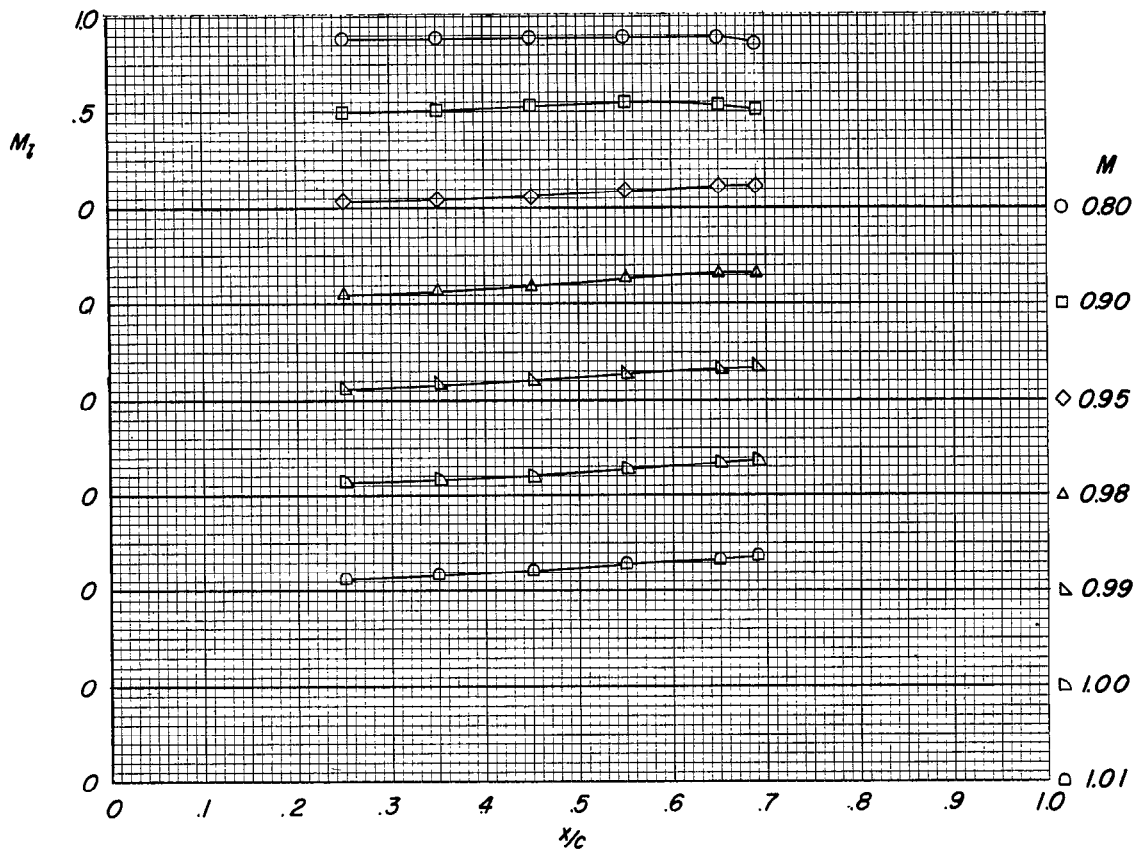
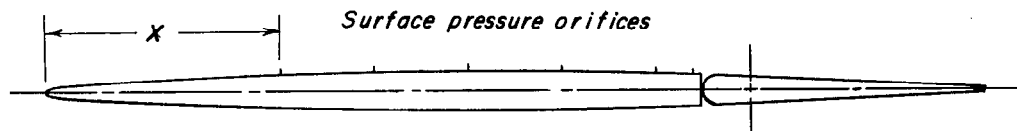


Figure 22.- Chordwise variation of local Mach number for various free-stream Mach numbers. $\alpha = 0^\circ$; $T = 0.17$.